CRISPRi-based screen of Autism Spectrum Disorder risk genes in microglia uncovers roles of *ADNP* in microglia endocytosis and uptake of synaptic material

Olivia M Teter[1,2], Nina M Dräger[1], Sydney M Sattler[1], Amanda McQuade[1], Brandon B Holmes[3], Vasileios Papakis[1,4], Kun Leng[1,5,6], Steven Boggess[1], David Shin[5,9], Tomasz J Nowakowski[7,8,9,10,11], James Wells[12], Martin Kampmann[1,13]

1 Institute for Neurodegenerative Diseases, University of California, San Francisco, San Francisco, CA, USA
2 UC Berkeley-UCSF Graduate Program in Bioengineering, University of California, San Francisco, San Francisco, CA, USA
3 Department of Neurology, University of California, San Francisco, CA, USA
4 Developmental and Stem Cell Biology Graduate Program, University of California, San Francisco, San Francisco, CA, USA
5 Biomedical Sciences Graduate Program, University of California, San Francisco, San Francisco, CA, USA
6 Medical Scientist Training Program, University of California, San Francisco, San Francisco, CA, USA
7 Department of Anatomy, University of California, San Francisco, San Francisco, CA 94158, USA
8 Department of Psychiatry and Behavioral Sciences, University of California, San Francisco, San Francisco, CA 94158, USA
9 Department of Neurological Surgery, University of California, San Francisco, San Francisco, CA 94158, USA
10 Weill Institute for Neurosciences, University of California, San Francisco, San Francisco, CA 94158, USA
11 Eli and Edythe Broad Center for Regeneration Medicine and Stem Cell Research, University of California, San Francisco, San Francisco, CA 94158, USA
12 Department of Pharmaceutical Chemistry, University of California, San Francisco, San Francisco, CA, USA
13 Department of Biochemistry and Biophysics, University of California, San Francisco, San Francisco, CA, USA

Abstract

Autism Spectrum Disorders (ASD) are a set of neurodevelopmental disorders with complex biology. The identification of ASD risk genes from exome-wide association studies and de novo variation analyses has enabled mechanistic investigations into how ASD-risk genes alter development. Most functional genomics studies have focused on the role of these genes in neurons and progenitor cells. However, roles for ASD risk genes in other cell types are largely uncharacterized. There is evidence from postmortem tissue that microglia, the resident immune cells of the brain, appear activated in ASD. Here, we systematically assess the impact of ASD-risk gene knock-down on microglial uptake of synaptic material. We developed both an iPSC-derived microglia-neuron coculture system and high-throughput flow cytometry readout for synaptic uptake to enable CRISPRi-based screening. Our screen identified *ADNP*, one of the high-confidence ASD risk genes, amongst others as a modifier of microglial synaptic uptake. Transcriptomic, proteomic, and functional analyses revealed that ADNP plays a role in endocytosis, cell surface remodeling, and motility in microglia. Through this focused investigation into the role of ADNP in microglia, we also found preliminary evidence for WNT signaling coordinating microglial uptake of synaptic material.

Introduction

Autism is a spectrum of neurodevelopmental disorders defined by core features, such as social and communication impairments and repetitive or restrictive behaviors. Although there is behavioral and etiological diversity – with both environmental and genetic factors contributing to ASD risk – there are shared patterns of atypical brain development including dysregulated synaptic density[1–3] and activation of microglia in people with ASD [4–8]. Microglia, the resident immune cells in the brain, play traditional immune regulatory roles as well as specialized roles to support circuit development including synaptic remodeling and regulation of neuronal activity[9–11]. It is not known if the observed activation of microglia in ASD is in response to abnormal neuronal cues or an intrinsic state of the microglia.

Given the complexity and multi-cellular coordination in these developmental processes, it is difficult to illuminate mechanisms underpinning how ASD risk factors give rise to atypical brain development. However, progress in genome sequencing and de novo mutation analyses have led to the identification of large effect size genes implicated in ASD risk[12]. Since the identification of these risk genes, CRISPR-based genetic screens in human iPSC-derived two- and three-dimensional neural cultures *in vitro*, as well as in mice have been conducted. These studies have focused on phenotypes in the neural lineage, including neurogenesis, neuronal migration and differentiation, and progenitor cell proliferation[13–18]. A subset of ASD risk genes are expressed, albeit not enriched, in microglia, and whether their expression is 'functional' is unknown. In this work, we explore how these risk genes act in microglia by using CRISPRi-based functional genomics to assess whether knocking down ASD risk genes in microglia can alter their ability to remodel synapses.

Towards this end, we developed a flow cytometry-based readout for one aspect of synaptic remodeling, uptake of synaptic material, using an engineered human iPSC-derived microglia-neuron coculture system. The development of this high-throughput synaptic pruning assay enabled us to conduct a pooled CRISPRi-based screen to assess if ASD risk genes modify microglial uptake of synaptic material. Our screen identified a subset of genes that modify this process including *ADNP*, one of the high-confidence ASD risk genes. Focused molecular and cellular characterization of iPSC-derived microglia (iTF-Microglia) with *ADNP* knockdown revealed that *ADNP* loss disrupts endocytosis, remodels the surface proteome, leads to inflammatory activation, and affects their motility and uptake of synaptic material. Through this focused investigation, we provide evidence that ASD risk genes can act directly in microglia to alter their activation state and interactions with neurons. We also provide preliminary evidence for WNT signaling as a signal coordinating synaptic remodeling.

Materials and methods

Human iPSC culture

iPSCs were cultured on Matrigel (Corning; Cat. No. 356231) coated vessels in StemFlex Media (Gibco; Cat. No. A3349401) until 80% confluent. Upon confluency, cells were washed with DPBS (Gibco; Cat. No. 14190-144), lifted using StemPro Accutase Cell Dissociation Reagent (GIBCO/Thermo Fisher Scientific; Cat. No. A11105-01) for 3 minutes at 37 ºC, diluted with DPBS, and pelleted by 5 minutes of centrifugation at 220g. The supernatant was aspirated, cells counted, resuspended in StemFlex supplemented with 10 µM Y-27632 dihydrochloride ROCK inhibitor (Tocris; Cat. No. 1254), and plated on Matrigel coated vessels. StemFlex was replenished daily.

Human iPSC-derived microglia (iTF-Microglia) with CRISPRi compatibility
iPSC-derived microglia (iTF-Microglia) were established by Draeger et al., 2022[19]. Briefly, iPSCs with stably integrated doxycycline-inducible transcription factors (PU1, CEBPβ, IRF5, MAFB, CEBPα, and IRF8) and Trimethoprim (TMP)-inducible CRISPRi machinery – hereafter referred to as 6TF-iPSCs – were kept according to the above procedure. At day 0, 6TF-iPSCs were replated onto Matrigel and PDL coated plates in Essential 8 Medium (Gibco; Cat. No. A1517001) supplemented with 10 µM ROCK inhibitor, 2 µg/mL doxycycline (Clontech; Cat. No. 631311), and 50 nM TMP (MP Biomedical; Cat. No. 195527). On day 2, the media was changed to Advanced DMEM/F12 Medium (Gibco; Cat. No. 12634-010) supplemented with 1□×□Antibiotic-Antimycotic (Anti-Anti) (Gibco; Cat. No. 15240-062), 1□×□GlutaMAX (Gibco; Cat. No. 35050-061), 2□µg/mL doxycycline, 50 nM TMP, 100□ng/mL Human IL-34 (Peprotech; Cat. No. 200-34) and 10□ng/mL Human GM-CSF (Peprotech; Cat. No. 300-03). On day 4, the media was changed to Advanced DMEM/F12 supplemented with 1□×□Anti-Anti, 1□×□GlutaMAX, 2□µg/mL doxycycline, 50 nM TMP, 100□ng/mL Human IL-34, 10□ng/mL, Human GM-CSF, 50□ng/mL Human M-CSF (Peprotech; Cat. No. 300-25), and 50□ng/mL Human TGFB1 (Peprotech; Cat. No. 100-21C). On day 8, the differentiated iTF-Microglia were used for assay or coculture.

Human iPSC-derived neuron (iNeuron) differentiation
iPSC-derived neurons (iNeurons) were established by Tian et al., 2019[20]. Briefly, iPSCs with stably integrated doxycycline-inducible NGN2 – hereafter referred to as NGN2-iPSC s – were kept according to the above procedure. On day -3, NGN2-iPSCs were replated onto Matrigel coated plates in Knockout DMEM/F-12 (Gibco; Cat. No. 12660012) supplemented with 1 x MEM Non-Essential Amino Acids Solution (Gibco; Cat. No. 11140-050), 1 x N2 supplement (Gibco; Cat. No. 17502-048), 10 ng/mL NT-3 (Peprotech; Cat. No. 450-03), 10 ng/mL BDNF (Peprotech; Cat. No. 450-02), 1 µg/mL mouse laminin (Gibco; Cat. No. 23017015), 10 µM ROCK inhibitor, and 2 µg/mL docycycline. On day -2, the cells were taken out of ROCK inhibitor by replacing the media with day –3 media formulation minus ROCK inhibitor. On day 0, the cells were washed with DPBS, lifted with Accutase, pelleted by 5 minutes of 300g centrifugation, and plated on PDL coated plates in BrainPhys Neuronal Medium (StemCell Technologies; Cat. No. 05790) supplemented with 0.5X N2 supplement, 0.5X B27 supplement (Gibco; Cat. No. 17504044), 10 ng/mL NT-3, 10 ng/mL BDNF, 1 µg/mL mouse laminin, and 2 µg/mL doxycycline. On day 3, the media was fully changed with day 0 media minus doxycycline. On day 7, half the media was removed and replaced by day 3 media.

iNeuron and iTF-microglia coculture
iNeurons and iTF-microglia were differentiated as described above. Day 8 iTF-microglia were washed with DPBS, lifted with TrypLE Express (Gibco; Cat. No. 12605-028) for 10 minutes at 37 ºC, diluted with Advanced DMEM/F-12, and pelleted by 8 minutes of 300g centrifugation. The supernatant was aspirated and the pellet was resuspended in day 0 neuronal media supplemented with 2X the cytokines and doxycycline used in day 4 microglia media. The iTF-microglia suspension was added to day 14 neurons to achieve a 10:3 (iNeuron:iTF-microglia) ratio in a half media change for a final concentration of 1X cytokines. Subsequent experiments occurred after three days of coculture.

Lentivirus preparation
HEK293T cells were plated in tissue culture plastic dishes in DMEM (Gibco; Cat. No. 10313-039) supplemented with 10% fetal bovine serum (Gibco; Cat. No. A3382001) and 1% Penicillin-Streptomycin (Gibco; Cat. No. 15140122). Once 80-95% confluent, the media was fully changed in preparation for transfection. The transfection mix was prepared by mixing equal parts transfer

DNA and Packaging Mix (0.8 µg psPAX2, 0.3ug pMD2G, 0.1 µg pAdVantage). This mixture was diluted with Opti-MEM I Reduced Serum Medium (Gibco; Cat. No. 31985070) before adding Lipofectamine 2000 Transfection Reagent (Invitrogen; Cat. No. 11668027). The solution incubated at room temperature for 10 minutes before being added to HEK293s. After two days, the media was taken up using a syringe and passed through a 0.45 µm filter. Lentivirus Precipitation Solution (Alstem; Cat. No. VC100) was added at a 1:4 (lentivirus precipitation solution:media) ratio, thoroughly mixed, and incubated at 4 ºC overnight. The virus was pelleted by 30 minutes of 1500g centrifugation at 4 ºC. The supernatant was removed and the pellet resuspended in DPBS.

Plasmid engineering

pKL078: pHIV CAG:Lck-mNeonGreen-P2A-NLS-mTagBFP2

pKL078 was prepared by ligating a gblock containing an Lck sequence and PCR amplified mNeonGreen and mTagBFP2 (Plasmid #55320) products into a lentivirus backbone using Gibson assembly as per the manufacturer's instructions.

pOT056: pCagg-Gamillus

pOT056 was prepared by PCR amplifying Gamillus (addgene plasmid #124837) and ligating it into a lentivirus backbone using Gibson assembly as per the manufacturer's instructions.

pOT020: pCagg-synaptophysin-Gamillus

pOT020 was prepared by PCR amplifying Gamillus (addgene plasmid #124837) and synaptophysin (addgene plasmid #119738) and ligating them into a lentivirus backboneusing Gibson assembly as per the manufacturer's instructions.

Membrane labeling of microglia

Lentivirus was prepared according to the above procedure for a pKL078. 6TF-iPSCs were kept according to the above procedure. Once confluent, the 6TF-iPSCs were washed with DPBS, lifted using Accutase for 3 minutes at 37 ºC, diluted with DPBS, and pelleted by 5 minutes of 220 g centrifugation. The supernatant was aspirated and the pellet was resuspended in StemFlex, 10 µM ROCK inhibitor, and lentivirus. The media was fully changed after two days. The transduced 6TF-iPSCs were expanded, sorted on green fluorescence using the BD FACSAria Fusion (BD Biosciences), and maintained to be used for live imaging of iTF-microglia. To compare the morphology of monoculture and coculture iTF-microglia, these labeled microglia were plated 10:3 with unlabeled:labeled iTF-microglia or iNeurons:labeled iTF-microglia.

Engineering neurons expressing Gamillus constructs

Lentivirus was prepared according to the above procedure for pOT056 and pOT020. NGN2-iPSCs were kept according to the above procedure. Once confluent, the NGN2-iPSCs were washed with DPBS, lifted using Accutase for 3 minutes at 37 ºC, diluted with DPBS, and pelleted by 5 minutes of 220 g centrifugation. The supernatant was aspirated and the pellet was resuspended in StemFlex, 10 µM ROCK inhibitor, and lentivirus. The media was fully changed after two days. The transduced NGN2-iPSCs were expanded, sorted on green fluorescence using the BD FACSAria Fusion (BD Biosciences), and maintained to be used for live synaptic uptake assays.

Quant-seq for characterization of iTF-microglia and iNeurons in coculture

Cocultures were prepared as previously described with membrane labeled iTF-Microglia. Cell culture media was aspirated, cells washed twice with Hank's Balanced Salt Solution (HBSS) (Gibco; Cat. No. 14025092), and lifted using Papain (Worthington Biochemical; Cat. No. LK003178) with 5 mM magnesium chloride and 5 µg/mL DNase (Worthington; Code: DPRF;

Cat. No. LS006333). After 10 minutes at 37 ºC, the papain was diluted with HBSS supplemented with 5 µg/mL DNAse and 5mM magnesium chloride. The lifted cells were pelleted at 300g for 8 minutes. The supernatant was aspirated and the pellet resuspended in HBSS supplemented with 5 µg/mL DNAse and 5 mM magnesium chloride and immediately moved to ice. The cocultures were sorted into separate microglia and neuron populations by FACS based on the mNeonGreen expressed by the microglia.

Monoculture neurons were prepared as previously described. To compare to the coculture neurons, the monoculture neurons received a media change at day 14 containing IL-34, GM-CSF, TGFB, M-CSF, and dox according to the coculture media. Similarly, monoculture microglia were prepared such that at day 8, the microglia were lifted with TryplE and replated in the coculture media on PDL plates.

RNA from biological duplicates for each condition (more than 30,000 cells for each sample) was extracted using the Quick-RNA Miniprep Kit (Zymo; Cat. No. R1055). Libraries were prepared from total RNA (15 ng per sample) using the QuantSeq 3′ mRNA-Seq Library Prep Kit for Illumina (FWD) (Lexogen; Cat. No. 015UG009V0252) following the manufacturer's instructions. Library amplification was performed with 17 total PCR cycles. mRNA-Seq library concentrations (mean of 5.36 ± 2.37 ng μl^{-1}) were measured with the Qubit dsDNA HS Assay Kit (Invitrogen; Cat. No. Q32851) on a Qubit 2.0 Fluorometer. Library fragment-length distributions (mean of 269 ± 18 base pairs) were quantified with High Sensitivity D5000 Reagents (Agilent Technologies; Cat. No. 5067-5593) on the 4200 TapeStation System. The libraries were sequenced on an Illumina NextSeq 2000 P2 instrument with single-end reads.

Transcripts were aligned to the human reference genome (GRCh38, release 42) using Salmon v.1.4.0[21] (the --noLengthCorrection, --validateMappings, --gcBias flags were used). Transcripts were mapped to genes and quantified using tximeta. To visualize gene expression for genes related to neurons, microglia, complement, and microglial activation, the row centered and scaled counts were displayed using Enhanced Heaptmap (gplots, version 3.1.3.1).

Flow cytometry assay for uptake of Gamillus protein

NGN2-iPSCs engineered with various gamillus constructs were differentiated according to the above protocol. 6TF-iPSCs were transduced with a non-targeting sgRNA that includes a nuclear BFP marker, differentiated, and cocultured with the aforementioned engineered neurons. After three days of coculture, the cells were washed with HBSS, lifted using Papain with 5 mM magnesium chloride and 5 µg/mL DNase for 10 minutes at 37 ºC, and diluted with HBSS. Single cell fluorescence was measured by flow cytometry using the BD FACS Celesta (BD Biosciences). Microglia uptake of gamillus was analyzed by measuring the median green fluorescence of the BFP+ population. For synaptic uptake experiments with pharmacological treatments, cocultures were treated with 200 nM Cytochalasin D (Invitrogen; Cat. No. PHZ1063). For Notum, day 12 neurons were treated with 100 ng/mL Notum (R&D Systems; Cat. No. 9118-NM) and treated again on day 14 with the addition of iTF-Microglia. For AnnexinV treatments, day 14 neurons were incubated with 1:100 AnnexinV (Invitrogen; A13202) for 15 minutes at 37 ºC, washed with HBSS, and replenished with neuron conditioned media before iTF-Microglia were added for coculture.

Library preparation and synaptic pruning screen

Top and bottom oligos for two sgRNAs targeting each of the 102 ASD-risk genes[12] and 28 non-targeting controls were ordered from IDT (Supplementary Table 1). Sequences were chosen according the two highest predicted activity scores from Horlbeck et al., 2016[22]. Top and bottom oligos were annealed then pooled before ligating into the sgRNA backbone, pMK1334[20], that

contains a nuclear BFP. Lentivirus was prepared according to the previously described protocol. 6TF-iPSCs were transduced with the library with MOI < 0.15, selected using 1 µg/mL Puromycin dihydrochloride (Sigma; Cat. No. P9620), and differentiated into microglia for coculture with iNeurons expressing synaptophysin-Gamillus. After 3 days of coculture, cells were washed with HBSS then lifted with Papain with 5 mM magnesium chloride and 5 µg/mL DNase for 10 minutes at 37 ºC. Cells were diluted with HBSS and pelleted before resuspension in HBSS with 5 mM magnesium chloride and 5 µg/mL DNase. Microglia (BFP+ cells) were sorted by FACS (BD FACSAria Fusion) into populations with low (bottom 25%) or high (top 25%) Gamillus-FITC signal. Low and high Gamillus-FITC samples from three replicates were prepared for next-generation sequencing as previously described[19]. Briefly, genomic DNA was isolated using a Macherey-Nagel Blood L kit (Macherey-Nagel; Cat. No. 740954.20) and sgRNA sequences were amplified and sequenced on an Illumina MiSeq V3.

Reads were cropped, aligned to an index reflecting the sgRNA library sequences, and quantified using Bowtie (version 0.12.9). sgRNA counts were then analyzed using our MAGeCK-iNC pipeline[20]. Briefly, phenotypes and p-values for each gene were calculated using a Mann-Whitney U-test, comparing the distribution of non-targeting control sgRNAs. Hit genes were determined based on a false discovery rate of 10%.

qPCR

To validate knockdowns for *ADNP* and *FZD2*, RNA was extracted using the Quick-RNA Microprep Kit (Zymo Research, Cat. No. R1050) with DNA digest. RNA was converted to cDNA using SensiFAST cDNA Synthesis Kit (Meridian Bioscience, Cat. No. BIO-65053). qPCR reactions were setup using SensiFAST SYBR Lo-ROX 2X Master Mix (Bioline; Cat. No. BIO-94005), custom qPCR primers from Integrated DNA Technologies used at a final concentration of 0.2µM, and 5 ng of cDNA. Reaction amplification was measured using the Applied Biosystems QuantStudio 6 Pro Real-Time PCR System using QuantStudio Real Time PCR software (v.1.3). Expression fold changes were calculated using the ΔΔCt method, normalizing to housekeeping gene *GAPDH*.

Primer description	Primer sequence (5'-3')
GAPDH qPCR for	ATGCCTCCTGCACCACCAAC
GAPDH qPCR rev	GGGGCCATCCACAGTCTTCT
ADNP qPCR for	GAGGATGTAGGACTGTGGGA
ADNP qPCR rev	TCTTCACTATGGACATTGCGG
FZD2 qPCR for	CTGCATGTCTACCAAGTACGT
FZD2 qPCR rev	GTGCCATCCTATCTCAGCTAC

Immunohistochemistry (IHC)

Cell cultures were first fixed using 4% paraformaldehyde (Electron Microscopy Sciences; Cat. No. 15710) for 15 minutes at room temperature. Cells were then washed thrice with DPBS before blocking and permeabilizing for one hour at room temperature with blocking buffer: DPBS supplemented with 5% Normal Goat Serum (Vector Laboratories; Cat. No. S-1000-20) with 0.01% Triton X-100 (TEKnova; Cat. No. T1105). Primary antibodies were diluted in blocking buffer and left at 4 ºC overnight. Samples were washed thrice with DPBS. Secondary antibodies were diluted in blocking buffer and added for 1-2 hours at room temperature. Secondary antibody solutions were washed thrice with DPBS before imaging using the Molecular Devices Image Express Confocal HT.ai or IN Cell Analyzer 6000 (GE; Cat. No. 28-9938-51).

Target	Dilution	Catalogue Number

Anti-ADNP	1:500 (IF), 1:1000 (WB)	Novus Biologicals; NBP1-89236
Anti-CLTC	1:500 (IF)	ProteinTech; 66487-1-Ig
Anti-Rab5A	1:200 (IF)	Cell signaling; 46449
Anti-Rab11A	1:200 (IF)	Invitrogen; MA5-49197
Anti-CD68	1:1000 (IF)	BioRad; MCA5709
Anti-GM130	1:500 (IF)	Abcam; ab169276
Anti-COL1A1	1:200 (IF)	Cell Signaling; 66948
Anti-α Tubulin	1:1000 (IF)	Cell Signaling; 3873
Anti-FZD2	1:500(IF)	ProteinTech; 24272-1-AP
Anti-NeuN	1:500 (IF)	Abcam; ab279296
Anti-GAPDH	1:50,000 (WB)	SCBT; sc-47724
Anti-vGlut1	1:500 (IF)	Sigma; MAB5502
Anti-Homer	1:500 (IF)	Synaptic Systems; 160003

Surveillance dynamics

Membrane labeled iTF-Microglia were cocultured with iNeurons. After three days of coculture, time lapse images were acquired using a 20X objective every 15 seconds for 30 minutes on an IN Cell Analyzer 6000 (GE; Cat. No. 28-9938-51). Images were then segmented on the membrane label using CellProfiler's IdentifyPrimaryObjects. Segmentations for a given field of view were stacked and stabilized using ImageJ. Individual cells from various fields were cropped for single cell analysis of total area surveilled which equated to total area of the segmentation stack's max projection normalized to initial cell area.

Phagocytosis assays with in-well controls

The sgRNA backbone, pMK1334[20], that contains a nuclear BFP was modified using Gibson assembly to create a backbone containing a nuclear mApple protein. A non-targeting control (NTC 2) protospacer sequence was ligated into the new nuclear mApple backbone and protospacer sequences targeting *ADNP* or *FZD2* were ligated into the nuclear BFP backbone. Uptake of synaptic material with the in-well NTC iTF-Microglia was conducted as previously described with the modification that half of the microglia in the well carried the NTC sgRNA with nuclear mApple and the other half a gene targeting sgRNA with nuclear BFP. A similar composition of microglia were plated in monoculture for phagocytosis of synaptosomes and fluorescent beads (Polysciences; Cat. No. 15702-10). Synaptosomes were prepared using iNeurons expressing the synaptophysin-Gamillus construct and SynPer (Thermo Scientific; Cat. No. 87793) following the manufacturer's protocol. Microglia were treated with 3 mg/mL of synaptosomes or 1:1,000 dilution of beads for 1 hour then lifted using TryplE for 10 minutes at 37 ºC. Single cell fluorescence was measured by flow cytometry using the BD FACS Celesta (BD Biosciences).

CRISPRi sgRNA ID	Protospacer
NTC 1	GGATCGCGTCTAGTGCAGAT
NTC 2	GGGGTGAGGGTCCAATTCGG
ADNP 1	GGTGGGAGAGGCGGCTTCAC
ADNP 2	GCGTCGAGCGGTGCAGACAA
FZD2 1	GCCGACCGCGGCAAGCAAGC
FZD2 2	GCAGGAGGACGCAGGCCTAG

CROPseq analysis
Single cell RNA-sequencing of iTF-Microglia with CRISPRi-based gene knockdowns of 53 ASD risk genes was conducted and analyzed according to the methods described in Dräger 2022[19]. In brief, Cell Ranger (v.5.0.1, 10X Genomics) was used for alignment to the GRCh38-3.0.0 reference genome and gene expression quantification. DemuxEM71 was used for sgRNA assignment. The resulting data represented 4,466 cells and an average of 17,120 reads per cell (Supplementary Figure 3A-D). Differential expression analysis comparing single cells with sgRNAs targeting *ADNP* to NTCs was performed using the resulting Seurat object and FindMarkers function.

Surface proteomics
Surface proteomics was performed according to the protocol established in Kirkemo et al., 2022[23]. In brief, cells were lifted using Versene for 10 minutes at 37 ºC. Cells were diluted in DPBS and pelleted by centrifugation at 1500 g for 5 minutes and resuspended in DPBS pH 6.5. Cell surfaces were labeled by incubating 0.5 µM of WGA-HRP for 5 minutes on ice, then adding 500 µM biotin tyramide, and finally adding 1 mM of H2O2. The mixture was incubated at 37 ºC for 2 minutes. The reaction was quenched with 10 mM Sodium Ascorbate/1 mM Sodium Pyruvate followed by two additional washes in the same buffer prior to a final wash in PBS. Cells were pelleted and flash frozen before mass spectrometry.

The cell pellet was thawed and processed for LC-MS/MS using a preOmics iST kit (P.O. 00027). Briefly, cell pellets were lysed in 2x RIPA buffer containing protease inhibitors (cOmplete, Mini, EDTA-free Protease Inhibitor Cocktail; Millipore Sigma 11836170001) and 1.25 mM EDTA. Cells were lysed via sonication. Biotinylated proteins were pulled down with NeutrAvidin-coated agarose beads (Thermo) for 1 hour at 4 °C. Beads were transferred to Poly-Prep chromatography columns (Bio-Rad) and sequentially washed with 1x RIPA buffer, high-salt PBS (PBS pH 7.4, 2 M NaCl [Sigma]), and denaturing urea buffer (50 mM ammonium bicarbonate, 2 M Urea). From the PreOmics iST kit, 50 µL of the provided LYSE solution was added to the slurry and the mixture was incubated at 55 °C for 10 minutes with shaking. The provided enzymes mixture (Trypsin and LysC) were resuspended in 210 µl of RESUSPEND buffer, mixed, and added to the slurry. Samples were allowed to mix at 500 rpm for 1.5 hours at 37 °C, before being quenched with 100 µl of STOP solution. Sample was spun in provided C18 spin cartridge and washed 1X with 200µl of WASH 1 and WASH 2. Peptides were eluted with 2X 100 µl of ELUTE, dried, and resuspended with 2% acetonitrile and 0.1% TFA. Peptides were quantified using Pierce Quantitative Colorimetric Peptide Assay (Thermo Fisher Scientific, 23275).

Mass spectrometry was performed as described previously in Kirkemo et al., 2022[23]. Briefly, 200 ng of samples were separated over a 90 minute 3%-35% ACN gradient on either an Aurora Ultimate CSI 25cm×75µm C18 (Ionopticks) or a PepSep XTREME 25 cm x 150 µm (Bruker) UHPLC column using a nanoElute UHPLC system (Bruker), and injected into a timsTOF pro mass spectrometer (Bruker). For database searching, peptides were searched using PEAKS Online X version 1.7 against both the plasma membrane annotated human proteome (Swiss-prot GOCC database, August 3, 2017 release). Enzyme specificity was set to trypsin + LysC with up to two missed cleavages. Cysteine carbamidomethylation was set as the only fixed modification; acetylation (N-term) and methionine oxidation were set as variable modifications. The precursor mass error tolerance was set to 20 PPM and the fragment mass error tolerance was set to 0.05 Da. Data was filtered at 1% for both protein and peptide FDR and triaged by removing proteins with fewer than 2 unique peptides. All mass spectrometry database searching

was based off of three biological replicates. Biological replicates underwent washing, labeling, and downstream LC-MS/MS preparation separately.

Viability assay
Live cell cultures were incubated with TO-PRO-3 (Invitrogen; Cat. No. T3605) and Hoechst 33342 (Thermo Fisher Scientific; Cat. No. H3570) at 37 ºC for 15 minutes. Cultures were then imaged and nuclei were classified using CellProfiler pipelines as live or dead with dead cells having a high average TO-PRO-3 intensity.

Western blotting
Cells were washed twice with cold DPBS then lysed using 1 X RIPA buffer (Abcam; Cat. No. 156034) with protease (Roche; Cat. No. 11836170001) and phosphatase inhibitors (Roche; Cat. No. 4906845001). Cells lysates were collected and centrifuged at max speed for 5 minutes at 4 ºC. Protein concentration of the supernatant was measured using a BCA Protein Assay Kit (Pierce; Cat. No. 23225). 10 µg of protein was mixed with 1 X Laemmli SDS-Sample buffer, Reducing (bioworld #10570021-2) and boiled for 5 minutes at 95 ºC. Denatured proteins were loaded into a 4-12% Bis-Tris polyacrylamide gel (Invitrogen; Cat. No. NP0336BOX) and run at 120 V for 1 hour. Proteins were transferred to a nitrocellulose membrane using BioRad Transblot Turbo Transfer System for 11 minutes at 25 V. Nitrocellulose membranes were blocked for 1 hour at room temperature with Intercept (PBS) blocking buffer (Licor; Cat. No. 927-70001). Primary antibodies diluted in Intercept (PBS) blocking buffer were added overnight at 4 ºC. Membranes were washed thrice with TBST. Secondary antibodies diluted in Intercept (PBS) blocking buffer were added for 2 hours at room temperature. Membranes were washed thrice with TBST before being imaged on a Licor Immunoblots.

Cell surface staining for flow cytometry
iTF-Microglia were washed with DPBS, lifted using Versene (Gibco; Cat. No. 15040066) for 10 minutes at 37 ºC, diluted with Advanced DMEM/F-12, and pelleted by centrifugation at 300g for 5 minutes. Cell pellets were moved to ice where they were resuspended in FACS buffer: DPBS with 0.5% Bovine serum albumin (Sigma; Cat. No. A7906), 0.5 mM EDTA (Invitrogen; Cat. No. 15-575-020), and 1:100 FC block (BD Biosciences; Cat. No. 564220) for 15 minutes. Conjugated CD38 antibody (R&D Systems; Cat. No. FAB2404P) diluted in FACS buffer was added to the cells for a final dilution of 1:200. After 30 minutes, cells were washed twice with FACS buffer before measurement by flow cytometry using the BD FACS Celesta (BD Biosciences).

Dextran endocytosis
pHrodo Red dextran10,000 MW (Invitrogen; Cat. No. P10361) was diluted 1:50 in day 4 microglia media, added to cell cultures, and incubated at 37 ºC for various times. For degradation experiments, dextran was incubated with cells for three hours before being removed, washed, and replaced by day 4 microglia media. After uptake incubation, iTF-Microglia were washed and lifted using TryplE at 37 ºC for 10 minutes. Cells were diluted in cold HBSS before measurement by flow cytometry using the BD FACS Celesta (BD Biosciences).

Cytokine immunoassay
Secreted proteins in iTF-Microglia conditioned media were measured using the Proteome Profiler Human Cytokine Array Kit (R&D Systems; Cat. No. ARY005B) following the manufacturer's protocol. Chemiluminescent images were acquired using ChemiDoc Touch Imaging System. Integrated pixel intensity for each dot was measured using ImageJ. Integrated pixel intensities for technical replicate dots were averaged before subtracting the background as measured by the integrated pixel intensity for negative dots.

TREM2 Homogeneous Time Resolved Fluorescence (HTRF) assay
TREM2 concentrations were measured using the HTRF Human TREM-2 Detection Kit (Revvity; Cat. No. 63ADK099PEG) following the manufacturer's instructions. Cell lysates were collected using 1 X RIPA buffer with protease and phosphatase inhibitors. Cell lysate and media TREM2 concentrations were determined according to standard curves prepared in the aforementioned RIPA buffer or unconditioned media, respectively.

Results

Developing a high-throughput, *in vitro* assay for iPSC-derived microglia (iTF-Microglia) uptake of synaptic material

To systematically assess the role of ASD-risk genes in microglial uptake of synaptic material, we conducted a CRISPRi-based screen in human iPSC-derived microglia (iTF-Microglia) cocultured with iPSC-derived neurons (iNeurons). The standard method for measuring uptake of synaptic material involves volumetric confocal microscopy and advanced image analysis techniques to count synaptic puncta colocalized within microglial lysosomes. This method is not compatible with performing a high-throughput CRISPRi-based screen, so we developed a flow cytometry-based readout for uptake of synaptic material (Figure 1A). First, we established a scalable and rapid coculture protocol such that iTF-Microglia and iNeuron interactions can be assessed within 17 days (Supplementary Figure 1A). The cocultured cells retain their identity and iTF-Microglia show a trend towards decreased activation as measured by RNA-Sequencing (Supplementary Figure 1B). Towards developing a readout for uptake of synaptic material within the coculture, iNeurons were engineered with a presynaptic protein, synaptophysin, linked to an acid-tolerant, green fluorescent protein, Gamillus, and iTF-Microglia were engineered with a nuclear blue fluorescent protein. Upon coculture, the microglia population can be identified based on high blue fluorescence and the green fluorescence associated with uptake of synaptophysin-Gamillus from neurons can be measured (Figure 1A).

We first characterized our proposed strategy by investigating neuronal expression of the synaptophysin-Gamillus. iNeurons engineered with synaptophysin-Gamillus were stained for a presynaptic protein, vGlut1, and a post-synaptic protein, Homer (Figure 1B). Correlation analysis indicated that synaptophysin-Gamillus better correlated with vGlut1 compared to Homer, suggesting a preferentially pre-synaptic localization of synaptophysin-Gamillus (Figure 1C). A limitation of this construct is that a portion of synaptophysin-Gamillus was localized to the neuronal soma. However, time lapse imaging revealed that some somatic synaptophysin-Gamillus puncta were trafficked down neurites (Supplementary video 1). Further, time lapse imaging of neurons expressing synaptophysin-Gamillus cocultured with membrane-labeled iTF-Microglia revealed uptake and internal trafficking of synaptophysin-Gamillus puncta by iTF-Microglia (Figure 1D,E).

To assess the selectivity for uptake of specific types of neuronal materials by iTF-Microglia using this strategy, we compared the uptake of fluorescent material in iTF-microglia cocultured with neurons expressing synaptophysin-Gamillus to those cocultured with neurons expressing untagged Gamillus, which shows a diffuse cytosolic localization (Figure 1F-H, Supplementary Figure 1C). The expression of the Gamillus protein as measured by total fluorescence intensity within the iNeurons did not differ between the two engineered iNeuron cultures (Figure 1G). After coculturing the two engineered iNeuron populations with iTF-Microglia and quantifying the uptake of fluorescent material by the iTF-Microglia, we saw a significantly greater uptake of

material from neurons expressing synaptophysin-Gamillus compared to cytosolic Gamillus, suggesting that iTF-microglia selectively take up synaptic material in our assay (Figure 1H). The uptake of cytosolic Gamillus may be attributed to the clearance of dead neurons by iTF-Microglia as we observe an increase in culture viability and decrease in cell counts upon coculture (Supplementary Figure 1D,E). Altogether, we designed, engineered, and characterized a high-throughput, in vitro assay to measure iTF-Microglia uptake of synaptic material to be used in a CRISPRi-based screen of ASD-risk genes.

CRISPRi-based screen of ASD risk genes in iTF-Microglia nominates gene knockdowns, including *ADNP*, that affect microglial uptake of synaptic material

Using our flow-cytometry readout for iTF-Microglia uptake of synaptic material, we conducted a CRISPRi-based screen of ASD risk genes in iTF-Microglia (Figure 2A). Many ASD risk genes are thought to be haploinsufficient[24–26] due to the evidence of increased burden of heterozygous de novo loss of function mutations, including protein truncating variants and deleterious missense variants. Therefore, targeting of these genes by CRISPRi, which results in a partial reduction in gene expression, more closely models a heterozygous loss of function than complete gene knockout. We delivered sgRNAs targeting 102 ASD risk genes[12] to iPSCs stably expressing the CRISPRi machinery[19] that were then differentiated into iTF-Microglia to produce microglia with knockdowns (KDs) of individual ASD risk genes. These microglia were cocultured with the iNeurons expressing synaptophysin-Gamillus. Using fluorescence-activated cell sorting (FACS), iTF-Microglia were then sorted out of coculture into two populations: one with high green fluorescence (top 25%) or high uptake of synaptophysin-Gamillus and one with low green fluorescence (bottom 25%) or low uptake of synaptophysin-Gamillus. By comparing the frequencies of cells expressing each sgRNA across the two populations as determined by next-generation sequencing and comparing them to non-targeting control sgRNAs (NTCs), we identified genes that significantly increased or decreased uptake of synaptic material when knocked down (Figure 2B,C). Notably, knockdown of *ADNP* (Supplementary Figure 2A,B) one of the high-confidence ASD risk genes, increased iTF-Microglia uptake of synaptic material (Figure 5C). Previous work has shown mice with haploinsufficient *Adnp* have decreased spine density and developmental delays[27–29]. In neurons, ADNP plays a role in processes including differentiation[30,31], microtubule stability[32,33], and neurite outgrowth[34] but little is known about the role ADNP plays in microglia and how it may affect uptake of synaptic material.

To characterize ADNP in iTF-Microglia, we analyzed the localization of ADNP in both iNeurons and iTF-Microglia (Figure 2D). Consistent with previous work, ADNP is localized in the nucleus and cytoplasm[35,36] of our iNeurons with about 90% of neurons positive for nuclear ADNP (Figure 2E). The localization of ADNP in iTF-Microglia differs from that of neurons, showing a strong extranuclear punctate pattern and a low percentage of microglia positive for nuclear ADNP. The localization difference persists when iNeurons and iTF-Microglia are cocultured (Supplementary Figure 2C,D). This distinctive ADNP pattern across iNeurons and iTF-Microglia motivated us to investigate cell-type specific functions of ADNP.

***ADNP* knockdown affects endocytosis in iTF-Microglia**

We first used an unbiased transcriptomic approach to understand how *ADNP* KD affects iTF-Microglia by identifying differentially expressed genes (DEGs) when comparing iTF-Microglia with *ADNP* KD to iTF-Microglia with NTCs (Figure 3A, Supplementary Figure 3A-D). Due to the difference in ADNP localization between neurons and microglia in both our iPSC-derived cultures, we first analyzed the DEGs in terms of their associations with subcellular structures using GO Cellular Component enrichment. We found that many genes upregulated in the iTF-Microglia with *ADNP* KD are related to endosomes and secretory granules as well as focal

adhesions (Figure 3B). We then performed pathway enrichment analysis for upregulated DEGs from primary human microglia from postmortem samples from individuals with ASD and neurotypical controls[37]. The most significant GO Cellular Component pathways upregulated in this dataset point to ribosomal subunits, nucleus, and, interestingly, focal adhesion and endosomal compartments (Supplementary Table 2, Figure 3C,D). The conservation of upregulated endosomal compartments between these two datasets suggests that changes in endosomal pathways in microglia may be a common feature in ASD patients, beyond those with *ADNP* loss of function.

To assess whether ADNP is localized to any of these structures, we co-stained iTF-Microglia for ADNP and markers of various endosomal structures including clathrin, early endosomes, recycling endosomes, lysosomes, and the Golgi apparatus (Figure 3E). Using correlation and overlap analyses, we found that much of ADNP co-localized with clathrin and early endosome markers, although there was overlap with the other endosomal structures as well (Figure 3F,G). We did not find high overlap with microtubules despite previous work identifying a microtubule binding domain in the ADNP protein (Supplementary Figure 3E-G). The transcriptional signature and colocalization analyses motivated us to explore whether *ADNP* KD affected endocytosis. We found iTF-Microglia with *ADNP* KD showed less endocytosis as measured by internalization of pHrodo-labeled dextran (Figure 3H,I). Altogether, our transcriptomic, localization, and functional assays suggest that *ADNP* loss affects endocytosis in iTF-microglia, possibly due to a direct role that ADNP plays in this process.

ADNP loss remodels cell-surface receptors and secreted proteins, activates microglia and selectively affects uptake of live synaptic material

Endocytosis is an important process for remodeling the plasma membrane. To evaluate whether decreased endocytosis in iTF-Microglia with *ADNP* KD affects the receptor composition of the plasma membrane, we performed surface proteomics for iTF-Microglia with *ADNP* KD or a NTC (Figure 4A). We identified few proteins differentially abundant at the cell surface, but those that were significantly increased at the surface of iTF-Microglia with *ADNP* KD, including CD38, are associated with an immune signature (Figure 4B). Notably, previous work from our lab identified CD38 as a top marker for LPS-activated microglia[19]. The identification of CD38 as one of the most significantly increased receptors at the cell surface of iTF-Microglia with *ADNP* KD motivated us to hypothesize that *ADNP* KD may cause a similarly activated phenotype. We validated the mass spectrometry finding using flow cytometry to measure surface labeling of CD38 (Figure 4 C,D) and then characterized the secretome of iTF-Microglia with *ADNP* KD using an arrayed cytokine immunoassay (Figure 4E, Supplementary Table 3). Compared to iTF-Microglia with NTC, iTF-Microglia with *ADNP* KD had elevated secretion of CCL1, CD40 ligand, C5, CXCL11, and IL-4. Elevated C5 and IL-4 have been found to be associated with ASD[38,39]. Another important receptor for microglial activation and uptake of synaptic material is TREM2. From the aforementioned transcriptomics, we saw increased levels of *TREM2* mRNA. Interestingly, we did not find an increase in TREM2 in cell lysates, but we did observe an increase in TREM2 in the culture supernatant using a Homogeneous Time Resolved Fluorescence (HTRF) TREM2 assay (Figure 4F). TREM2 release from microglia is hypothesized to reflect activated TREM2 signaling[40]. Further comparing the transcriptomic data to the surface proteomics data (Supplementary Figure 4A) and the transcriptomic data to the secreted protein data (Supplementary Figure 4B), we saw no overlap in significantly differentially expressed genes and proteins but consistent trends across transcriptomic and proteomics for many genes and proteins of interest, suggesting that changes in the cell surfaceome were due to a combination of transcriptional and post-transcriptional mechanisms.

We next hypothesized that this activated profile would lead to a general increase in phagocytosis by iTF-Microglia with *ADNP* KD. However, when comparing uptake of fluorescent beads and synaptosomes derived from iNeurons expressing synaptophysin-Gamillus, we see no difference between iTF-Microglia with *ADNP* KD and iTF-Microglia with NTC in the same well (Figure 5A,B). We did validate our initial CRISPRi-based screen results showing iTF-Microglia with *ADNP* KD take up more synaptic material compared to iTF-Microglia with NTC when cocultured with iNeurons expressing synaptophysin-Gamillus (Figure 5C). The difference in phagocytosis between the synaptosomes and synaptic material in coculture led us to hypothesize that the iTF-Microglia with *ADNP* KD do not differentially recognize synaptic material but may take up more synaptic material in coculture because they are more motile and able to find more substrate. To test this hypothesis, we developed a live cell imaging pipeline in which we labeled the membranes of iTF-Microglia using an Lck-mNeonGreen transgene, acquired time lapses, segmented individual microglia, and compared the total area surveilled by the microglia to its initial area (Figure 5D). Comparing iTF-Microglia with *ADNP* KD to iTF-Microglia with NTC in monoculture, we saw no difference in surveillance area (Figure 5E). Interestingly, comparing the microglia in coculture, we saw that iTF-Microglia with *ADNP* KD had a larger surveillance area than iTF-Microglia with NTC (Figure 5F). The difference in surveillance area was not driven by differences in microglia morphology in monoculture or coculture (Supplementary Figure 5). In summary, iTF-Microglia with *ADNP* KD showed increased abundance of cell surface proteins associated with the immune system, increased secretion of CCL1, CD40 ligand, C5, CXCL11, IL-4, and TREM2, and increased uptake of synaptic material in coculture that was accompanied by increased motility.

Interfering with WNT signaling components can modulate iTF-Microglia uptake of live synaptic material

In order to take up synaptic material, microglia must migrate to and respond to secreted cues from neurons. We wondered if our difference in motility was due to differential sensing of neuronal ligands. Interestingly, our previous transcriptomic analyses uncovered “beta-catenin-independent WNT signaling” as one of the Reactome terms enriched among genes induced by knockdown of *ADNP* in iTF-Microglia (Figure 3B). Previous work in various cell types has shown that beta-catenin-independent WNT signaling, or non-canonical WNT signaling, can act as a signal for cell polarity and migration[41–43]. This observation motivated us to ask if WNT signaling may mediate interactions between microglia and neurons in coculture. Towards answering this question, we first checked the expression of Frizzled (FZD) receptors, the family of receptors that bind to WNT ligands, in monoculture and coculture iTF-Microglia by RNA-Sequencing (Figure 6A). We observed that FZD receptors have varied expression in iTF-Microglia and only *FZD2* is upregulated in coculture iTF-Microglia. Our surface proteomics dataset did not capture any FZD receptors, so we used an antibody staining approach to assess FZD2 protein levels. When we stained for and quantified FZD2 in cocultures with iTF-Microglia with *ADNP* KD or NTC, we saw increased FZD2 intensity within iTF-Microglia with *ADNP* KD (Figure 6B,C). To test the functional significance of FZD2 in the cocultured microglia, we compared uptake of synaptic material for iTF-Microglia with *FZD2* KD to iTF-Microglia with NTC and found that iTF-Microglia with *FZD2* KD (Supplementary Figure 6A) took up less synaptic material, suggesting that FZD2 may play a role in iTF-Microglia uptake of synaptic material (Figure 6D). To further investigate the contribution of WNT signaling to uptake of synaptic material, we treated cocultures with Notum, an enzyme that inactivates WNT ligands by removing their palmitoleic acid lipid modification (Figure 6E). Our cocultured iNeurons express several WNT ligands as measured by RNA-Sequencing, including *WNT4* and *WNT7B* which appear to be developmentally regulated in human and mouse transcriptomic datasets (Supplementary Figure 6B). Cocultures treated with Notum showed a decrease in iTF-Microglia uptake of synaptic material that was comparable to the decrease in uptake when cocultures were treated with

saturating concentrations (Supplementary Figure 6C-E) of Annexin V, a previously established blocker of phosphatidylserine and synaptic pruning[44] (Figure 6F). Altogether, we hypothesize that WNT signaling through microglial FZD2 helps coordinate microglial motility and uptake of synaptic material and that ADNP facilitates receptor recycling, including that for FZD2, such that knockdown of ADNP sensitizes microglia to WNT signaling (Figure 6G).

Discussion

In this study, we developed an iPSC-derived microglia-neuron coculture and flow cytometry method for measuring microglia uptake of synaptic material, which enabled us to conduct a CRISPR-based screen to systematically assess the effect of ASD-risk genes on microglial uptake of synaptic material. Recently published work presented a similar flow cytometry method for measuring microglial uptake of Alexa Fluor-labeled retinal ganglion cell (RGC) material in the lateral geniculate nucleus (LGN) after optic nerve crush[45]. Synapse remodeling of RGC inputs in the LGN is well defined such that internalization of Alexa Fluor-labeled material by microglia in the LGN can be attributed to synapse remodeling[11]. Since synapse remodeling is less understood *in vitro*, we designed the synaptophysin-Gamillus construct to provide greater insight into uptake of synaptic material compared to general neuronal material. This engineered platform can be used to assess uptake of synaptic material with other genetic perturbations, such as knockdown of genes associated with other neurodevelopmental or neurodegenerative disorders, in microglia and neurons or pharmacological perturbations.

Through this screen, we nominated ASD risk genes that affect microglia uptake of synaptic material. We further investigated the role of *ADNP*, a gene that when knocked down in microglia leads to increased uptake of synaptic material. Through transcriptomic, proteomic, and functional characterization of microglia with *ADNP* knockdown, we uncovered that loss of *ADNP* resulted in decreased endocytosis and increased motility in microglia. A previous study showed microglia activation following shRNA-mediated knockdown of *ADNP* with AAV9 delivery in mice[29]. AAV9 selectively infects neural cells, so subsequent microglia activation is induced in a cell non-autonomous manner. This microglia activation in response to *ADNP* knockdown in neural cells included increased microglia density, increased CD68 staining, and increased complement components[29]. From our work and others, we see that ADNP is expressed more highly in neurons than in microglia, and it is thus likely that a large contribution to autism phenotypes is due to neuronal dysfunction; however, microglia dysregulation is commonly seen in ASD patient brain tissue, and mechanisms regulated by low level expression of ASD risk proteins in microglia could contribute. Our work supports this idea and adds to our understanding of the biology of ADNP syndrome by investigating the specific effect of *ADNP* loss in microglia. We offer evidence that ADNP and perhaps other ASD risk genes can induce an activated microglia state in a cell-autonomous manner.

We also provide preliminary evidence for WNT signaling playing a role in the uptake of synaptic material. Recent work has provided evidence for WNT signaling by microglia coordinating retraction of astrocytic processes from synapses to promote synaptic remodeling in a whisker deprivation paradigm[46]. Our data offers a complimentary yet new insight into the role of WNT signaling between neurons and microglia. In the past several years, many studies have revealed that microglia can sense previously characterized neuronal signaling cues like purines, GABA, and neuromodulators like serotonin and use those signals to instruct motility, synaptic shielding, and synaptic remodeling[35]. Based on our work, we hypothesize that WNT ligands, used in axonogenesis and synaptogenesis[47–49], may stand as another neuronal signaling cue that microglia sense and respond to.

In summary, we used CRISPRi-based screen to systematically knock down 102 ASD risk genes in iPSC-derived microglia and a high-throughput flow cytometry method to measure uptake of synaptic material. This functional genomics approach allowed us to nominate ASD risk genes that affect this phenotype and consider synaptic remodeling as a point of mechanistic convergence by which some of these ASD risk genes act. A limitation to our approach is the physiological relevance of uptake of synaptic material in an iPSC-derived microglia-neuron coculture. Many studies of uptake of synaptic material by microglia in *in vivo* mouse models investigate well characterized periods of activity-dependent synaptic remodeling. However, our system reproduces key aspects conserved in *in vivo* assays, such as decreased uptake of synaptic material by blocking phosphatidylserine[44,50], suggesting principles of synaptic material uptake by microglia may hold true in our experimental paradigm.

Data availability
All datasets will be made available at NCBIGeo at the time of publication.

Code availability
All code, including R notebooks for transcriptomic analyses and CellProfiler pipelines for image analyses, will be made available at https://kampmannlab.ucsf.edu/resources at the time of publication.

Acknowledgements
We thank Ilana Gozes for advice and insights into studying *ADNP*, Caroline Mrejen for sharing her microscopy expertise, Sarah Elmes for sharing her flow cytometry and FACS expertise. We are grateful to the Autism Brain Net team for providing access to postmortem human brain tissue. We thank Nawei Sun and Jeremy Willsey for sharing sgRNA oligos. We acknowledge and thank all members of the Kampmann lab for their technical support and positive scientific community. This work was supported by the National Science Foundation Graduate Research Fellowship under Grant No. (NSF grant no. 2034836, to O.T.), and NIH/NIMH grant U01 MH115747 (to M.K.), R01 MH125516 (to T.J.N.).

Author Contributions
The CRISPRi-based screen was designed, conducted, and analyzed by OT and MK. The CROP-Sequencing experiment was conducted and analyzed by ND, SS, and OT. ADNP follow up experiments were conducted by OT with BH leading the design, experiment, and analysis of surface proteomics and AM contributing to the TREM2 experiment design and analysis. DS shared human brain tissue. Wnt experiments were conducted by OT. OT, VP, KL, and SB contributed to cloning efforts. OT and MK created the figures and wrote the manuscript with contributions from AM. All authors reviewed and approved the final manuscript.

Competing Interests
M.K. is a co-scientific founder of Montara Therapeutics and serves on the Scientific Advisory Boards of Engine Biosciences, Casma Therapeutics, Cajal Neuroscience, Alector, and Montara Therapeutics, and is an advisor to Modulo Bio and Recursion Therapeutics. M.K. is an inventor on US Patent 11,254,933 related to CRISPRi and CRISPRa screening, and on a US Patent application on *in vivo* screening methods.

References
1. Hutsler, J. J. & Zhang, H. Increased dendritic spine densities on cortical projection neurons in autism spectrum disorders. *Brain Res.* **1309**, 83–94 (2010).

2. Tang, G. *et al.* Loss of mTOR-Dependent Macroautophagy Causes Autistic-like Synaptic Pruning Deficits. *Neuron* **83**, 1131–1143 (2014).
3. Penzes, P., Cahill, M. E., Jones, K. A., VanLeeuwen, J.-E. & Woolfrey, K. M. Dendritic spine pathology in neuropsychiatric disorders. *Nat. Neurosci.* **14**, 285–293 (2011).
4. Morgan, J. T. *et al.* Microglial Activation and Increased Microglial Density Observed in the Dorsolateral Prefrontal Cortex in Autism. *Biol. Psychiatry* **68**, 368–376 (2010).
5. Tetreault, N. A. *et al.* Microglia in the Cerebral Cortex in Autism. *J. Autism Dev. Disord.* **42**, 2569–2584 (2012).
6. Suzuki, K. *et al.* Microglial Activation in Young Adults With Autism Spectrum Disorder. *JAMA Psychiatry* **70**, 49 (2013).
7. Voineagu, I. *et al.* Transcriptomic analysis of autistic brain reveals convergent molecular pathology. *Nature* **474**, 380–384 (2011).
8. Nardone, S. *et al.* DNA methylation analysis of the autistic brain reveals multiple dysregulated biological pathways. *Transl. Psychiatry* **4**, e433–e433 (2014).
9. Weinhard, L. *et al.* Microglia remodel synapses by presynaptic trogocytosis and spine head filopodia induction. *Nat. Commun.* **9**, 1228 (2018).
10. Miyamoto, A. *et al.* Microglia contact induces synapse formation in developing somatosensory cortex. *Nat. Commun.* **7**, 12540 (2016).
11. Schafer, D. P. *et al.* Microglia Sculpt Postnatal Neural Circuits in an Activity and Complement-Dependent Manner. *Neuron* **74**, 691–705 (2012).
12. Satterstrom, F. K. *et al.* Large-Scale Exome Sequencing Study Implicates Both Developmental and Functional Changes in the Neurobiology of Autism. *Cell* **180**, 568-584.e23 (2020).
13. Jin, X. *et al.* In vivo Perturb-Seq reveals neuronal and glial abnormalities associated with autism risk genes. *Science* **370**, eaaz6063 (2020).

14. Meng, X. *et al.* Assembloid CRISPR screens reveal impact of disease genes in human neurodevelopment. *Nature* **622**, 359–366 (2023).
15. Li, C. *et al.* Single-cell brain organoid screening identifies developmental defects in autism. *Nature* **621**, 373–380 (2023).
16. Sun, N. *et al.* Autism genes converge on microtubule biology and RNA-binding proteins during excitatory neurogenesis | bioRxiv. https://www.biorxiv.org/content/10.1101/2023.12.22.573108v2.
17. Lalli, M. A., Avey, D., Dougherty, J. D., Milbrandt, J. & Mitra, R. D. High-throughput single-cell functional elucidation of neurodevelopmental disease–associated genes reveals convergent mechanisms altering neuronal differentiation. *Genome Res.* **30**, 1317–1331 (2020).
18. Cederquist, G. Y. *et al.* A Multiplex Human Pluripotent Stem Cell Platform Defines Molecular and Functional Subclasses of Autism-Related Genes. *Cell Stem Cell* **27**, 35-49.e6 (2020).
19. Dräger, N. M. *et al.* A CRISPRi/a platform in human iPSC-derived microglia uncovers regulators of disease states. *Nat. Neurosci.* **25**, 1149–1162 (2022).
20. Tian, R. *et al.* CRISPR Interference-Based Platform for Multimodal Genetic Screens in Human iPSC-Derived Neurons. *Neuron* **104**, 239-255.e12 (2019).
21. Patro, R., Duggal, G., Love, M. I., Irizarry, R. A. & Kingsford, C. Salmon provides fast and bias-aware quantification of transcript expression. *Nat. Methods* **14**, 417–419 (2017).
22. Horlbeck, M. A. *et al.* Compact and highly active next-generation libraries for CRISPR-mediated gene repression and activation. *eLife* **5**, e19760 (2016).
23. Kirkemo, L. L. *et al.* Cell-surface tethered promiscuous biotinylators enable comparative small-scale surface proteomic analysis of human extracellular vesicles and cells. *eLife* **11**, e73982 (2022).
24. Iossifov, I. *et al.* The contribution of de novo coding mutations to autism spectrum disorder. *Nature* **515**, 216–221 (2014).

25. Deciphering Developmental Disorders Study. Prevalence and architecture of de novo mutations in developmental disorders | Nature. https://www.nature.com/articles/nature21062.
26. McCarthy, S. E. *et al.* De novo mutations in schizophrenia implicate chromatin remodeling and support a genetic overlap with autism and intellectual disability. *Mol. Psychiatry* **19**, 652–658 (2014).
27. Hacohen-Kleiman, G. *et al.* Activity-dependent neuroprotective protein deficiency models synaptic and developmental phenotypes of autism-like syndrome. *J. Clin. Invest.* **128**, 4956–4969 (2018).
28. Sragovich, S. *et al.* The autism-mutated ADNP plays a key role in stress response. *Transl. Psychiatry* **9**, 235 (2019).
29. Conrow-Graham, M. *et al.* A convergent mechanism of high risk factors ADNP and POGZ in neurodevelopmental disorders. *Brain* **145**, 3250–3263 (2022).
30. Sun, X., Peng, X., Cao, Y., Zhou, Y. & Sun, Y. ADNP promotes neural differentiation by modulating Wnt/β-catenin signaling. *Nat. Commun.* **11**, 2984 (2020).
31. Mandel, S., Spivak-Pohis, I. & Gozes, I. ADNP differential nucleus/cytoplasm localization in neurons suggests multiple roles in neuronal differentiation and maintenance. *J. Mol. Neurosci. MN* **35**, 127–141 (2008).
32. Ivashko-Pachima, Y. *et al.* SH3- and actin-binding domains connect ADNP and SHANK3, revealing a fundamental shared mechanism underlying autism. *Mol. Psychiatry* **27**, 3316–3327 (2022).
33. Oz, S. *et al.* The NAP motif of activity-dependent neuroprotective protein (ADNP) regulates dendritic spines through microtubule end binding proteins. *Mol. Psychiatry* **19**, 1115–1124 (2014).

34. Ganaiem, M., Karmon, G., Ivashko-Pachima, Y. & Gozes, I. Distinct Impairments Characterizing Different ADNP Mutants Reveal Aberrant Cytoplasmic-Nuclear Crosstalk. *Cells* **11**, 2994 (2022).
35. Gozes, I. ADNP Regulates Cognition: A Multitasking Protein. *Front. Neurosci.* **12**, 873 (2018).
36. Bennison, S. A. *et al.* The cytoplasmic localization of ADNP through 14-3-3 promotes sex-dependent neuronal morphogenesis, cortical connectivity, and calcium signaling. *Mol. Psychiatry* **28**, 1946–1959 (2023).
37. Gandal, M. J. *et al.* Broad transcriptomic dysregulation occurs across the cerebral cortex in ASD. *Nature* **611**, 532–539 (2022).
38. Fagan, K., Crider, A., Ahmed, A. O. & Pillai, A. Complement C3 Expression Is Decreased in Autism Spectrum Disorder Subjects and Contributes to Behavioral Deficits in Rodents. *Mol. Neuropsychiatry* **3**, 19–27 (2017).
39. Than, U. T. T. *et al.* Inflammatory mediators drive neuroinflammation in autism spectrum disorder and cerebral palsy. *Sci. Rep.* **13**, 22587 (2023).
40. Filipello, F. *et al.* Soluble TREM2: Innocent bystander or active player in neurological diseases? *Neurobiol. Dis.* **165**, 105630 (2022).
41. Hu, D. J.-K., Yun, J., Elstrott, J. & Jasper, H. Non-canonical Wnt signaling promotes directed migration of intestinal stem cells to sites of injury. *Nat. Commun.* **12**, 7150 (2021).
42. Čapek, D. *et al.* Light-activated Frizzled7 reveals a permissive role of non-canonical wnt signaling in mesendoderm cell migration. *eLife* **8**, e42093 (2019).
43. Chae, W.-J. & Bothwell, A. L. M. Canonical and Non-Canonical Wnt Signaling in Immune Cells. *Trends Immunol.* **39**, 830–847 (2018).
44. Scott-Hewitt, N. *et al.* Local externalization of phosphatidylserine mediates developmental synaptic pruning by microglia. *EMBO J.* **39**, e105380 (2020).

45. Dissing-Olesen, L. *et al.* FEAST: A flow cytometry-based toolkit for interrogating microglial engulfment of synaptic and myelin proteins. *Nat. Commun.* **14**, 6015 (2023).
46. Faust, T. E. *et al.* Microglia-astrocyte crosstalk regulates synapse remodeling via Wnt signaling. *bioRxiv* 2024.02.08.579178 (2024) doi:10.1101/2024.02.08.579178.
47. Lucas, F. R. & Salinas, P. C. WNT-7a induces axonal remodeling and increases synapsin I levels in cerebellar neurons. *Dev. Biol.* **192**, 31–44 (1997).
48. Ahmad-Annuar, A. *et al.* Signaling across the synapse: a role for Wnt and Dishevelled in presynaptic assembly and neurotransmitter release. *J. Cell Biol.* **174**, 127–139 (2006).
49. Sahores, M., Gibb, A. & Salinas, P. C. Frizzled-5, a receptor for the synaptic organizer Wnt7a, regulates activity-mediated synaptogenesis. *Dev. Camb. Engl.* **137**, 2215–2225 (2010).
50. Morizawa, Y. M. *et al.* Synaptic pruning through glial synapse engulfment upon motor learning. *Nat. Neurosci.* **25**, 1458–1469 (2022).

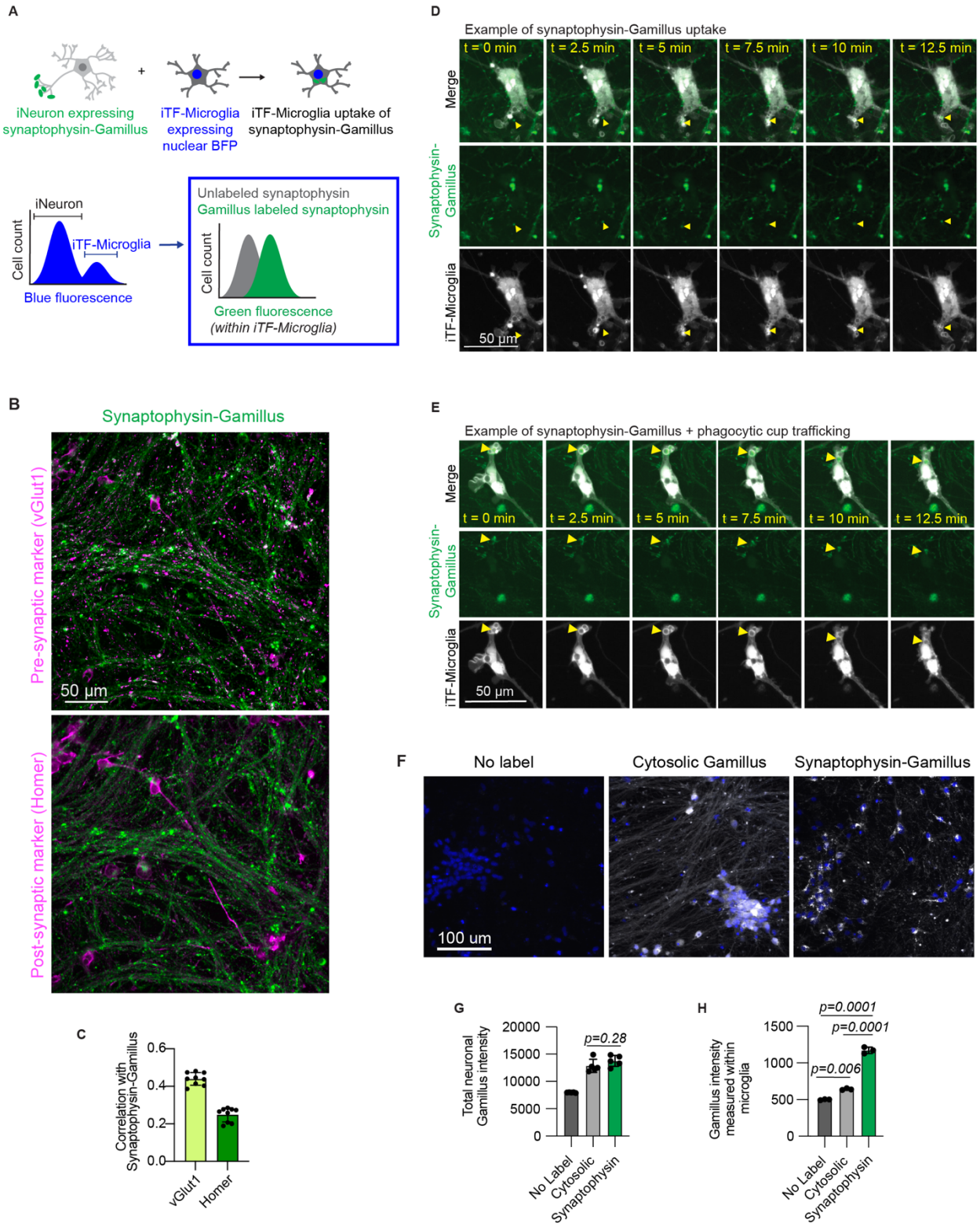

Figure 1: iPSC-derived microglia (iTF-Microglia) and iPSC-derived neuron (iNeuron) coculture enables monitoring of microglial uptake of synaptic material. A. Experimental and analytical strategy for measuring iTF-Microglia uptake of synaptic material from iPSC-derived neurons (iNeurons) using flow cytometry. (Top) iNeurons are engineered to express

synaptophysin linked to the acid-tolerant green fluorescent protein, Gamillus. iTF-Microglia are engineered to express a nuclear blue fluorescent protein. (Bottom) After coculture and measurement using flow cytometry, iTF-Microglia are identified by their blue fluorescence, and the amount of green fluorescence from uptake of synaptophysin-Gamillus is measured within this iTF-Microglia population. B. Representative micrographs of iNeurons expressing synaptophysin-Gamillus (green) costained with an antibody against a presynaptic marker, vGlut1 (magenta, top), or a post-synaptic marker, Homer (magenta, bottom). C. Correlation analysis of synaptophysin-Gamillus with vGlut1 or Homer (N = 3 fields of view from 3 wells, bars represent mean +/- standard deviation). D,E. Time lapse images of iNeurons expressing synaptophysin-Gamillus (green) and iTF-Microglia expressing a membrane marker, Lck-mApple (gray). D. The yellow arrow highlights a synaptophysin-Gamillus punctum that is taken up into a phagocytic cup and beginning to be trafficked toward the iTF-Microglia's soma. E. The yellow arrow highlights a synaptophysin-Gamillus puncta inside a phagocytic cup that is being trafficked toward the iTF-Microglia's soma. F. Representative micrographs of iNeurons engineered to express cytosolic Gamillus or synaptophysin-Gamillus. Nuclei are marked by Hoechst 33342 and displayed in blue. Gamillus is displayed in gray. G. Expression of the Gamillus protein measured by total fluorescence intensity per field of view (n = 5 wells, bars represent mean +/- standard deviation, Tukey's multiple comparisons test). H. Uptake of Gamillus by iTF-Microglia in coculture measured by flow cytometry (n = 3 wells, bars represent mean +/- standard deviation, Tukey's multiple comparisons test).

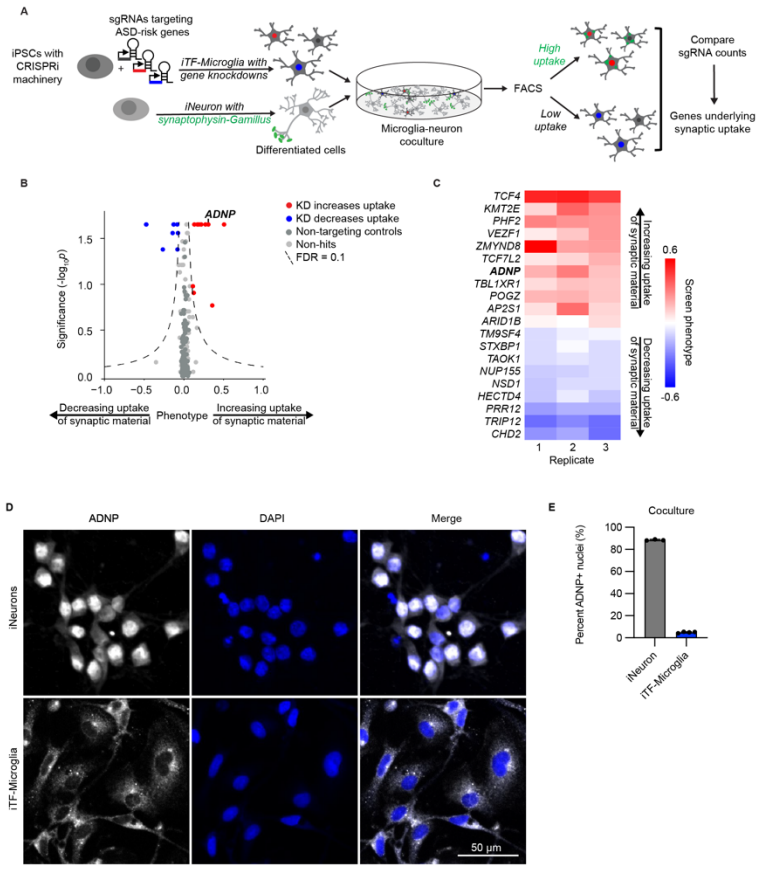

Figure 2: CRISPRi-based screen of ASD risk genes in iPSC-derived microglia (iTF-Microglia) nominates genetic knockdowns, including *ADNP*, that affect microglial uptake

of synaptic material. A. CRISPRi-based screening strategy to assess the role of ASD risk genes in microglial uptake of synaptic material. B. Volcano plot showing the effect of gene knockdowns in iTF-Microglia on uptake of synaptic material across three screening replicates and their corresponding statistical significance (two-sided Mann–Whitney U-test, false discovery rate (FDR) = 0.1). Gene knockdowns that increase uptake are noted in red, gene knockdowns that decrease uptake are noted in blue, non-targeting controls are noted in light gray, and non-hit gene knockdowns are noted in dark gray. C. Heatmap showing the phenotype of all gene knockdowns with a significant effect across three replicates of the screen. Gene knockdowns that increase uptake are noted in red, gene knockdowns that decrease uptake are noted in blue. D. Representative micrographs of iNeurons and iTF-Microglia showing the localization of ADNP (detected by immunofluorescence, gray) with respect to nuclei demarked by Hoechst 33342 (blue). E. Quantification of the percent of nuclei with high ADNP intensity (N = 3-4 wells per cell type, bars represent mean +/- standard deviation).

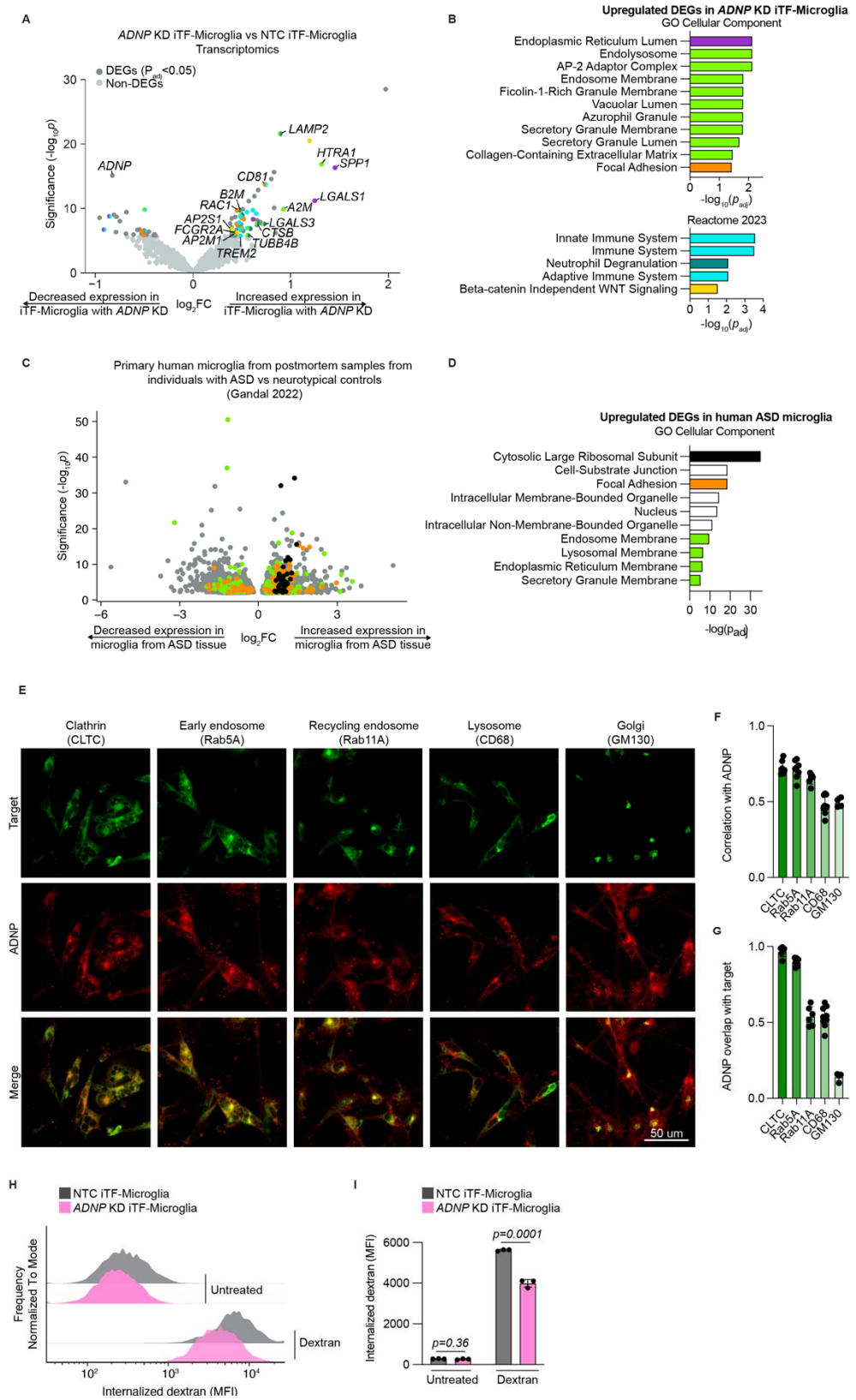

Figure 3: *ADNP* knockdown affects endocytosis in iPSC-derived microglia (iTF-Microglia). A. Volcano plot showing the change in expression as measured by RNA-sequencing for individual genes in iTF-Microglia with *ADNP* knockdown (KD) compared to iTF-Microglia with

non-targeting control (NTC) sgRNAs. RNA-sequencing data extracted from a CROP-seq dataset, see Methods for detail. Significantly differentially expressed genes (DEGs) are noted in dark gray or color-coded based on their corresponding categorization in enrichment analyses (B) and genes with no statistically significant change are noted in light gray (DEGs, Padj < 0.05, two-tailed Student's t-test). B. GO term Cellular Component and Reactome 2023 enrichment analyses of DEGs with increased expression in iTF-Microglia with *ADNP* KD. Terms representing unique gene sets and with Padj < 0.05 are displayed. Terms are color-coded such that terms of the same color have many overlapping genes. C. Volcano plot showing the change in expression as measured by single cell RNA-sequencing for DEGs in microglia from postmortem tissue from individuals with ASD compared to neurotypical controls[37] (DEGs, Benjamini & Hochberg corrected p values < 0.01). D. GO term Cellular Component enrichment analyses of DEGs with increased expression in microglia from postmortem tissue from individuals with ASD. Terms representing unique gene sets and with Padj < 0.05 are displayed. Terms are color-coded such that terms of the same color have many overlapping genes. E. Representative immunofluorescence micrographs of iTF-Microglia stained with antibodies against ADNP (red) and various endolysosomal organelle markers including CLTC, Rab5A, Rab11A, CD68, and GM130 (green). F. Average Pearson correlation between ADNP and individual organelle markers measured per cell for a given field of view (N = 1-4 fields of view from 3 wells, bars represent mean +/- standard deviation). G. Average Mander's overlap for ADNP and individual organelle markers measured per cell for a given field of view (N = 1-4 fields of view from 3 wells, bars represent mean +/- standard deviation). H. Quantification of endocytosis by dextran uptake. Representative histograms from flow cytometry measurements of iTF-Microglia with *ADNP* KD or NTC incubated with pHrodo dextran (10kDa) for 2 hours. I. Median fluorescence intensity (MFI) from internalized dextran (N = 3 wells, bars represent mean +/- standard deviation, multiple t-tests).

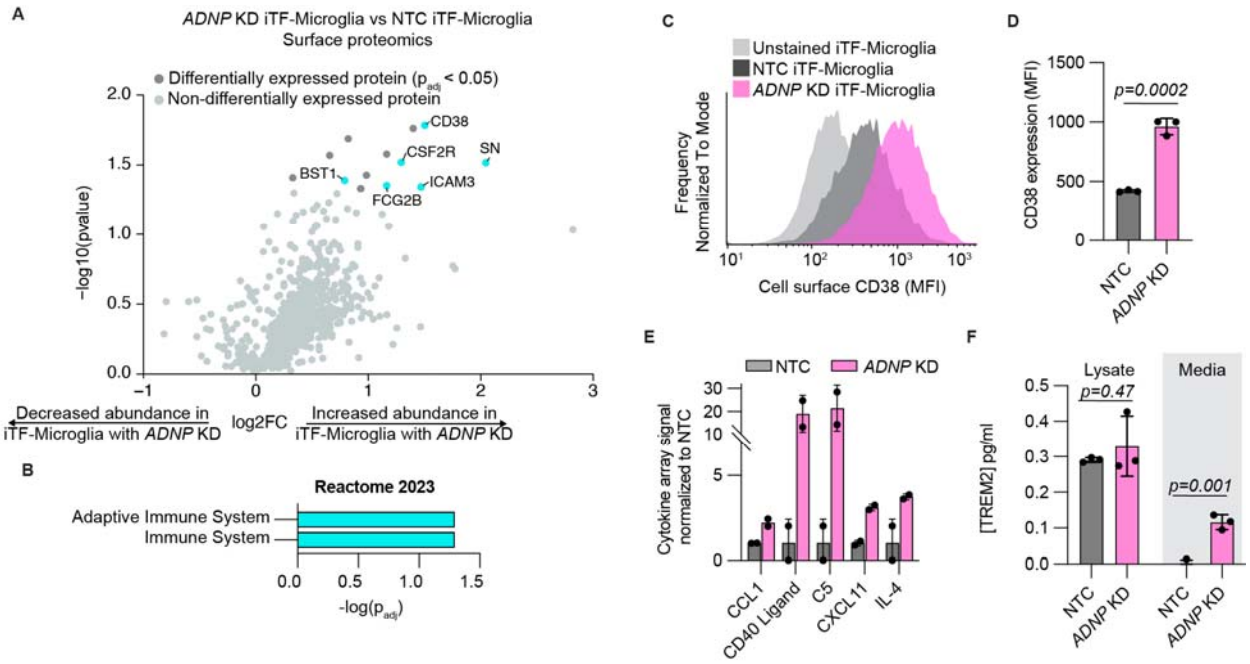

Figure 4: *ADNP* loss remodels cell-surface receptors and secreted proteins. A. Volcano plot showing the change in abundance for individual surface proteins in iPSC-derived microglia (iTF-Microglia) with *ADNP* knockdown (KD) compared to iTF-Microglia with non-targeting control (NTC) sgRNA as determined by surface protein labeling and mass spectroscopy (N = 3 replicates per cell type). Proteins with increased abundance in iTF-Microglia with *ADNP* KD are noted in dark gray or cyan based on their categorization in enrichment analyses (B) and proteins with no statistically significant change are noted in light gray (Differentially expressed proteins (DEPs), Padj < 0.05, two-tailed Student's t-test). B. Reactome enrichment analysis of proteins with increased abundance in iTF-Microglia with *ADNP* KD. C. Representative histograms from flow cytometry measurements of unstained iTF-Microglia and iTF-Microglia with *ADNP* KD or NTC stained for cell surface CD38. D. Median fluorescence intensity (MFI) from cell surface CD38 (N = 3 biological replicates, bars represent mean +/- standard deviation, t-test). E. Relative abundances measured using the integrated intensity from a cytokine array for proteins that have a trend for differential abundance between iTF-Microglia with NTC or *ADNP* KD (N = 2 wells, bars represent mean +/- standard deviation). F. TREM2 concentration of cell lysates or media collected from iTF-Microglia with *ADNP* KD or NTC measured using a Homogeneous Time Resolved Fluorescence (HTRF) assay (N = 3 wells, bars represent mean +/- standard deviation, t-test).

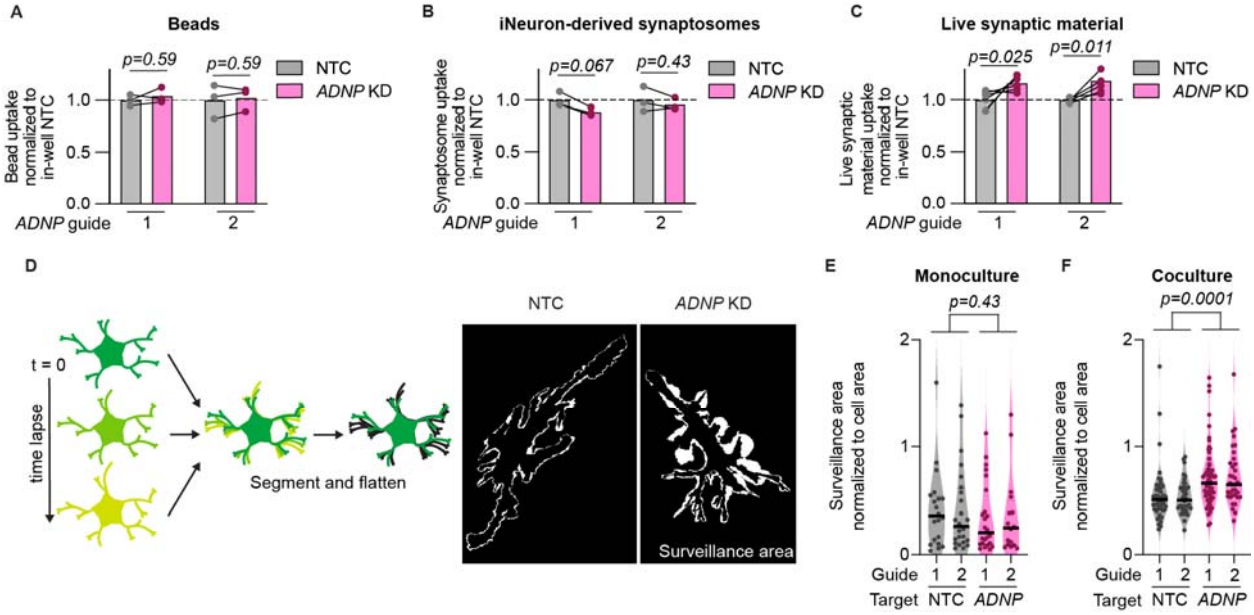

Figure 5: *ADNP* loss selectively affects uptake of live synaptic material. A-C. Uptake of various substrates by iTF-Microglia with *ADNP* KD or NTC measured by flow cytometry for bead (A) and iPSC-derived neuron (iNeuron)-derived synaptosome (B) uptake (N = 3 wells) and for live synaptic material (C) (N = 6 wells, multiple paired t-tests). D (Left) Surveillance area quantification strategy. Time lapse immunofluorescence micrographs of iTF-Microglia expressing a fluorescently tagged membrane protein, Lck-mNeonGreen, are acquired, segmented, and maximum-intensity projections are analyzed to measure surveillance area. (Right) Representative surveillance areas from coculture iTF-Microglia with *ADNP* KD or NTC. E. Single cell surveillance area normalized to initial cell area for monoculture iTF-Microglia with *ADNP* KD or NTC (N = 16-24 single cells, violin plot area represents the density curve, significance based on NTC vs ADNP factor computed by two-way ANOVA). F. Single cell surveillance area normalized to initial cell area for cococulture of iTF-Microglia with *ADNP* KD or NTC with iNeurons (N = 35-59 single cells, violin plot area represents the density curve, t significance based on NTC vs ADNP factor computed by two-way ANOVA).

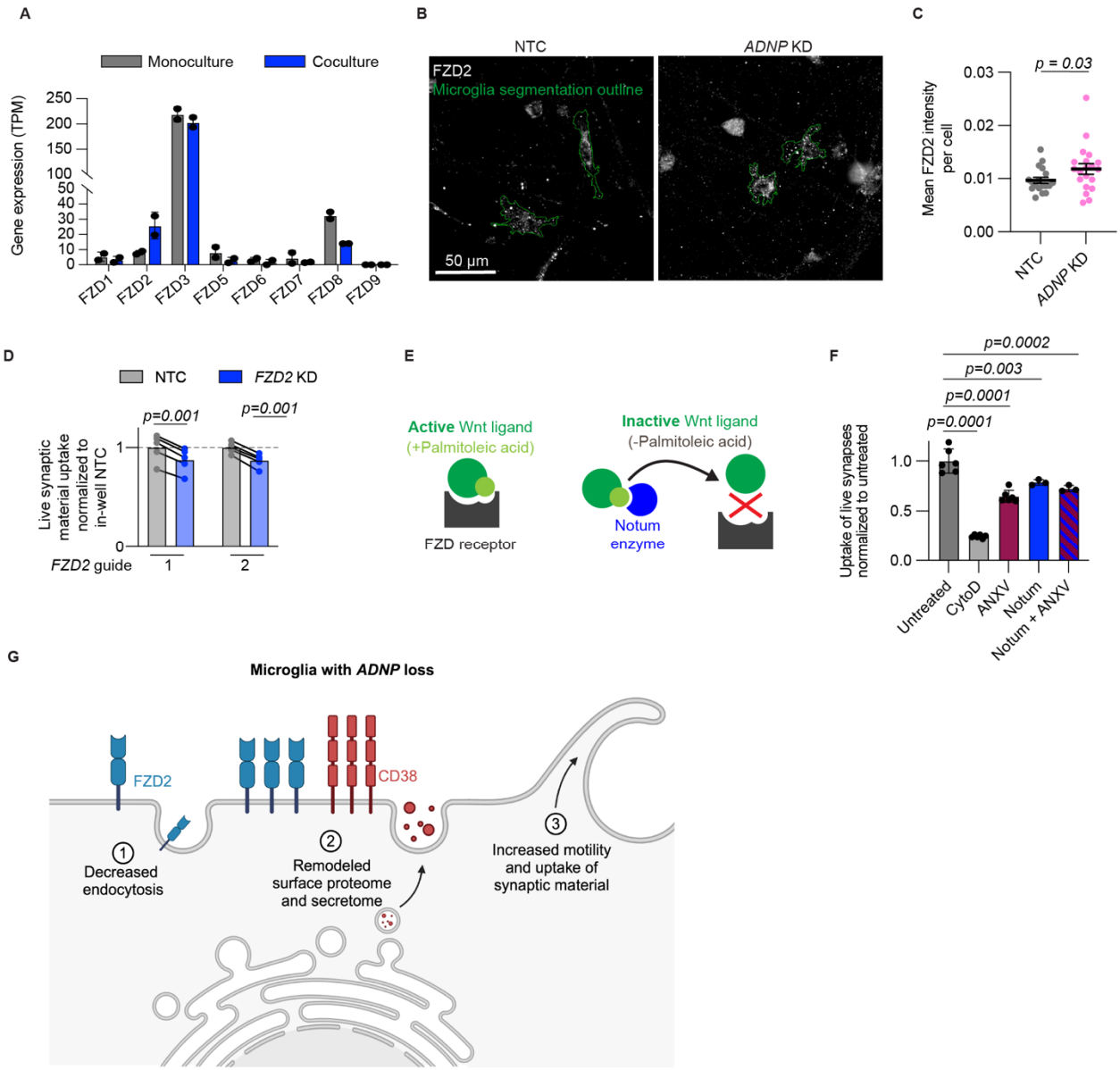

Figure 6: Interfering with WNT signaling can modulate iPSC-derived microglia (iTF-Microglia) uptake of live synaptic material. A. Gene expression measured by transcripts per million (TPM) for Fzd receptors in iTF-Microglia in monoculture and iNeuron coculture (N = 2 replicates, bars represent mean +/- standard deviation). B. Representative immunofluorescence micrographs of cocultures with iTF-Microglia with *ADNP* KD or NTC stained with an antibody against FZD2 (gray). iTF-Microglia in the cocultures expressed a fluorescently tagged membrane protein, Lck-mNeonGreen, that was used for segmentation (overlaid green outline). C. Mean FZD2 intensity per iTF-Microglia with *ADNP* KD or NTC (N = 17-20 single cells, t-test). D. Uptake of synaptic material by iTF-Microglia with *FZD2* KD or NTC (N = 5 wells, multiple paired t-tests). E. Mechanism of WNT interference by Notum. Notum depalmitoleylates WNT ligands which prevents binding to FZD receptors. F. Uptake of synaptic material by iTF-Microglia in cocultures with treatments including 200 nM cytochalasin D, Annexin V neuronal treatment, and 100 ng/mL Notum for three days (N = 3-6 replicates, Tukey's multiple comparisons test). G.

Hypothesized mechanism by which WNT signaling modulates iTF-Microglia uptake of synaptic material in coculture and how *ADNP* KD affects this process.

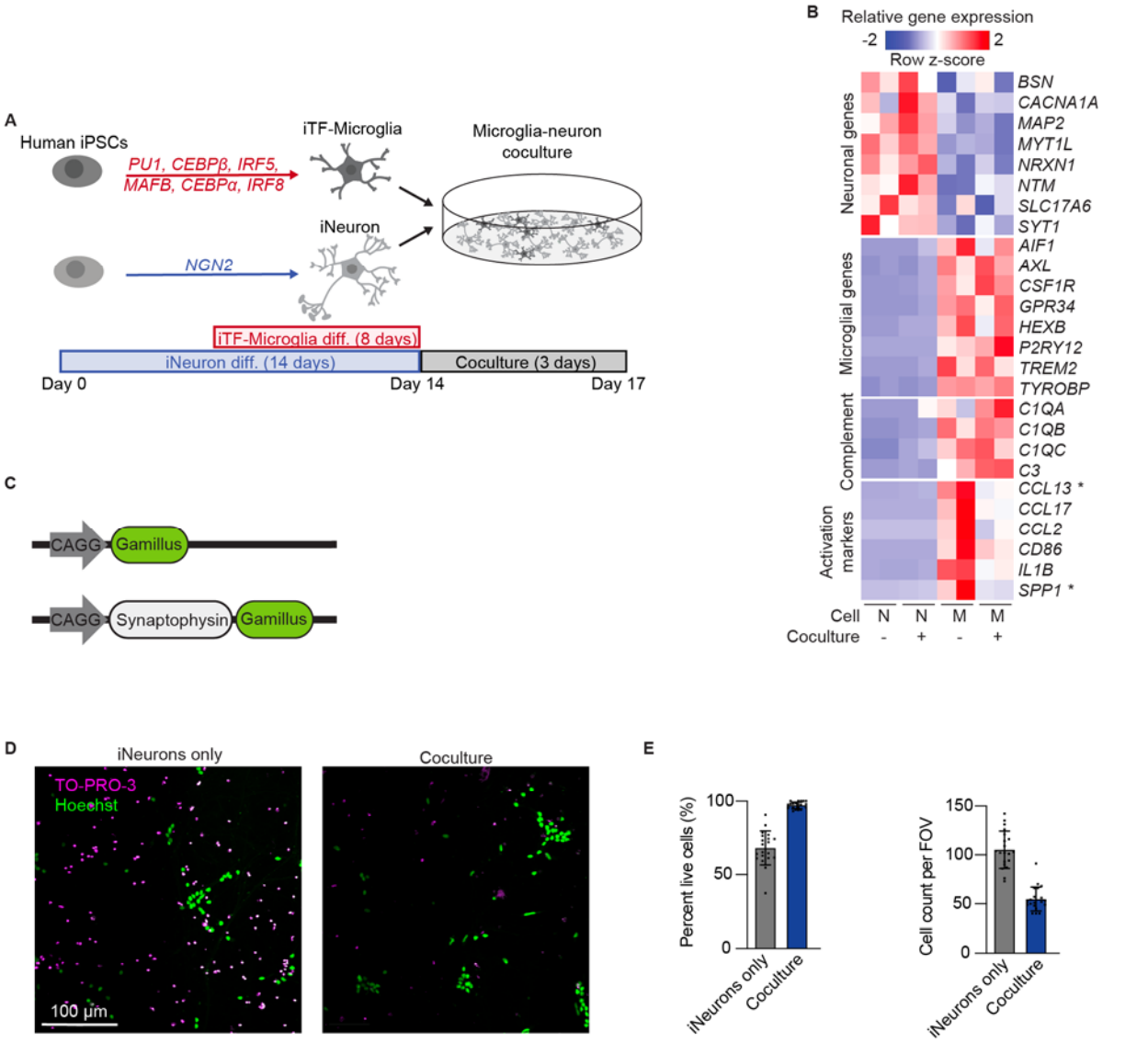

Supplementary Figure 1: Characterization of cocultures of iPSC-derived neuron (iNeuron) and iPSC-derived microglia (iTF-Microglia) and synaptic material uptake. A. iTF-Microglia and iNeuron differentiation and coculture strategy. B. Heatmap showing relative gene expression from RNA sequencing of neuronal genes, microglial genes, complement components, and microglial activation markers by iTF-Microglia (M) and iNeurons (N) in monoculture and coculture preparations (N = 2 biological replicates). C. Gamillus expression constructs for cytosolic Gamillus (top) and synaptophysin linked to Gamillus (bottom). D. Representative micrographs iNeuron monocultures (left) and iTF-Microglia and iNeuron coculture (right) stained with the dead cell indicator, TO-PRO-3 (magenta), and nuclear stain, Hoechst 33342 (green). E. (Left) Percent live cells based on nuclear TO-PRO-3 intensity (N = 4 fields of view (FOV) for 5 wells, bars represent mean +/- standard deviation). (Right) Total cell count per field of view based on nuclear Hoechst segmentations (N = 4 fields of view for 5 wells, bars represent mean +/- standard deviation).

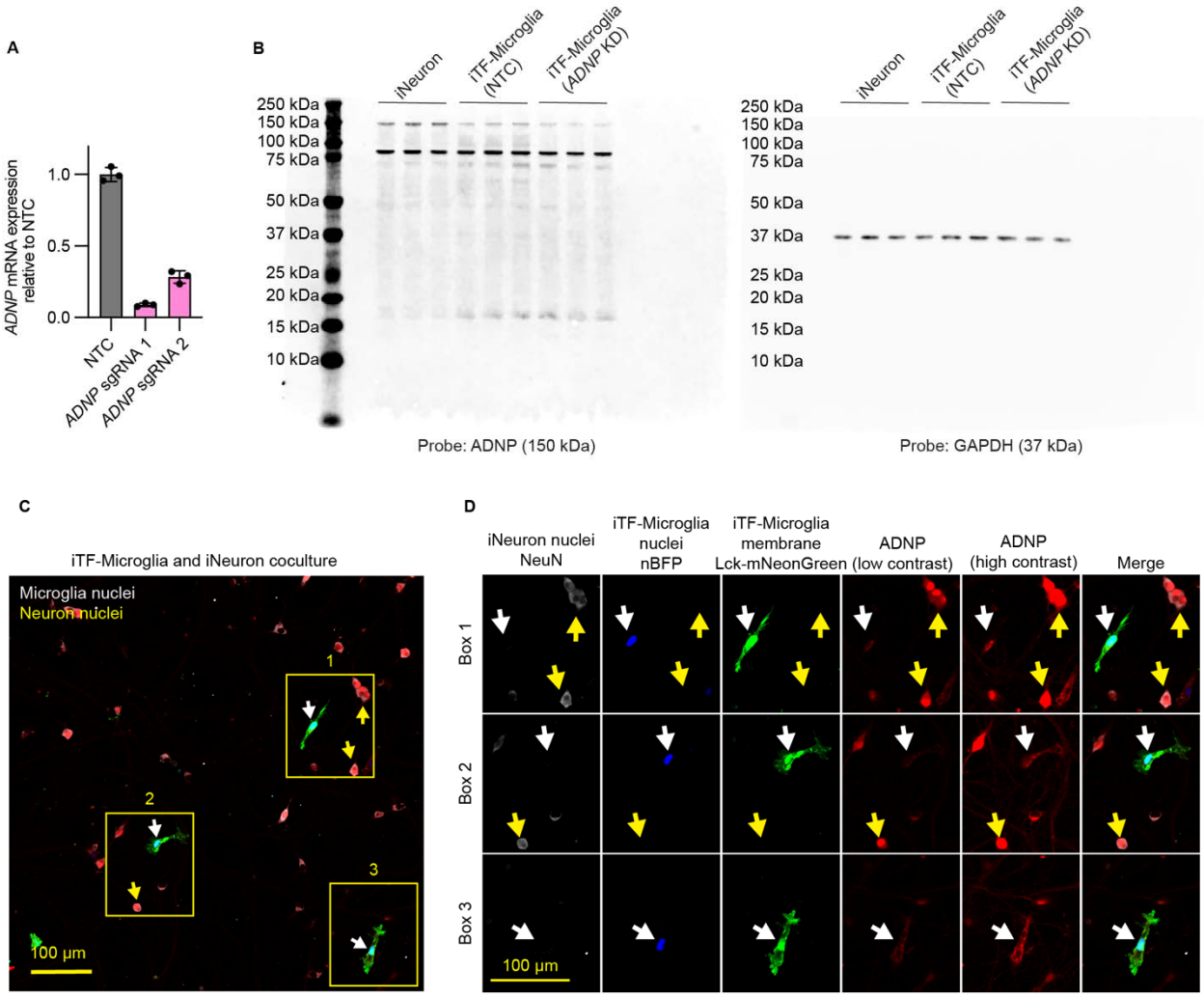

Supplementary Figure 2: ADNP antibody and localization validation. A. *ADNP* mRNA expression in iTF-Microglia with sgRNAs targeting *ADNP* or non-targeting control (NTC) measured by qPCR. B. Raw western blot images for ADNP stain (left) and GAPDH (right) for iPSC-derived neurons (iNeurons), iTF-Microglia with NTC, and iTF-Microglia with *ADNP* knockdown (N = 3 replicates per cell type). C. Representative micrograph of iPSC-derived microglia (iTF-Microglia) expressing membrane marker, Lck-mNeonGreen (green) and nuclear BFP (blue), and iNeuron coculture stained with NeuN (gray) and ADNP (red). White arrows indicate microglia and yellow arrows indicate neurons that are shown magnified. D. Insets and individual channels visualizing three iTF-Microglia in the coculture and their ADNP expression.

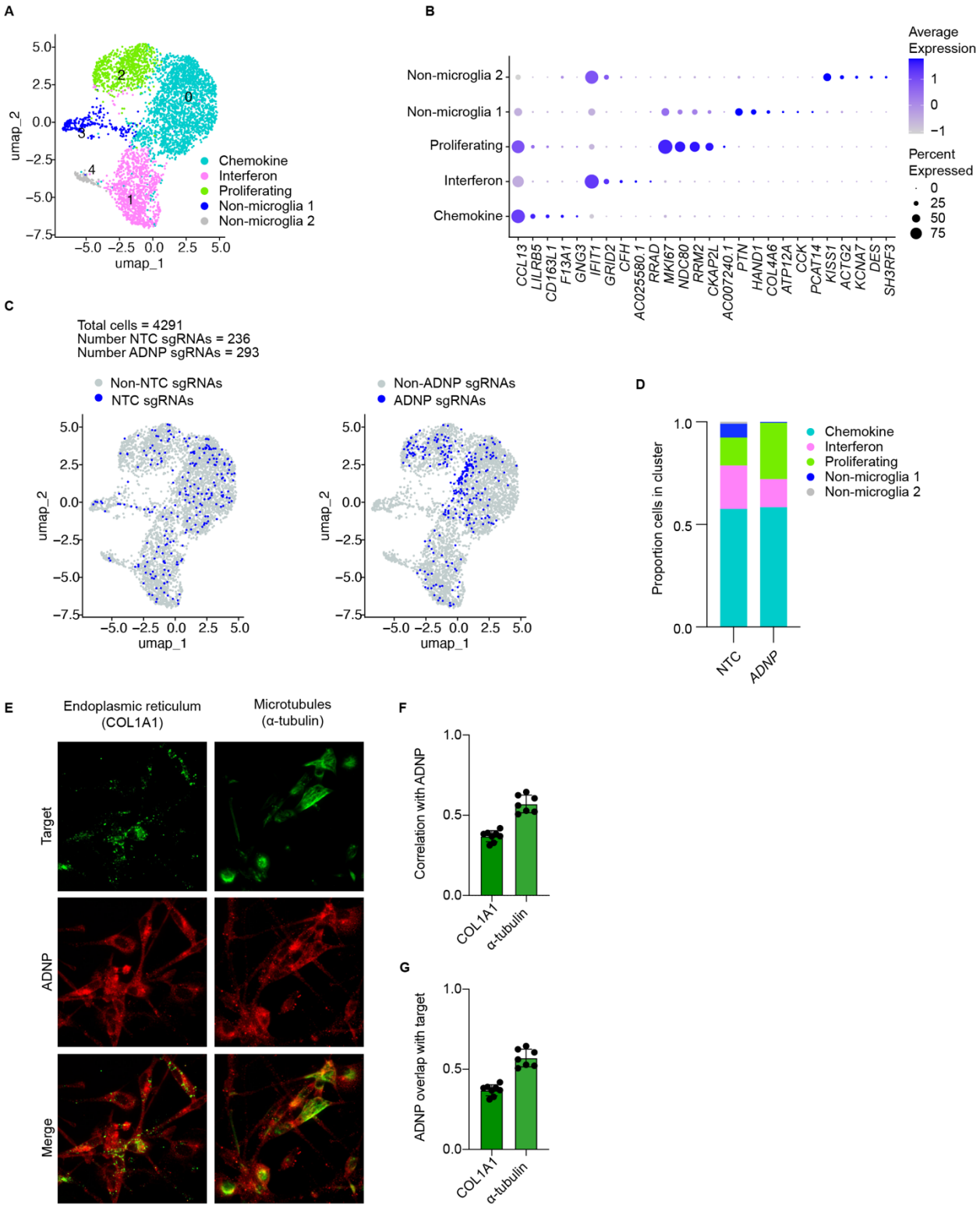

Supplementary Figure 3: Single-cell RNA sequencing analysis of iPSC-derived microglia (iTF-microglia). A. UMAP showing 5 clusters made up of iTF-Microglia with ASD risk gene knockdowns or non-targeting controls. B. Top 5 differentially expressed genes for each cluster conferring their associated descriptions: chemokine (CCL13 high), interferon (IFIT1 high),

proliferating (MKI67 high), and non-microglia states. C. Distribution of cells with non-targeting control sgRNAs (NTCs) (left) or ADNP targeting sgRNAs (right). D. Cluster occupancy as measured by proportion of cells in each cluster for iTF-Microglia with NTC sgRNAs or *ADNP* targeting sgRNAs. E. Representative immunofluorescence micrographs of iTF-Microglia stained with antibodies against ADNP (red) and against various organelles markers including α-tubulin and COL1A1 (green). F. Average Pearson correlation between ADNP and individual organelle markers measured per cell for a given field of view (N = 1-4 fields of view from 3 wells, bars represent mean +/- standard deviation). G. Average Mander's overlap for ADNP and individual organelle markers measured per cell for a given field of view (N = 1-4 fields of view from 3 wells, bars represent mean +/- standard deviation).

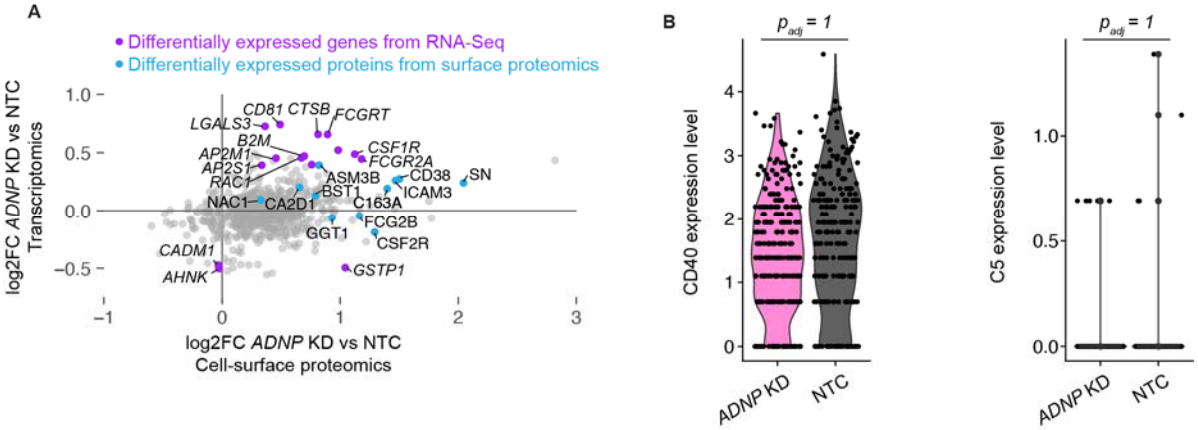

Supplementary Figure 4: Comparing the effect of *ADNP* knockdown on transcriptomics and cell-surface proteomics. A. Scatterplot showing the $\log_2$ fold change between iPSC-derived microglia (iTF-Microglia) with *ADNP* knockdown (KD) and iTF-Microglia with non-targeting control (NTC) for mRNA and surface protein abundances for genes that were identified in both transcriptomic and cell-surface proteomics datasets. Genes that were differentially expressed in the single-cell RNA sequencing dataset are noted in purple and labeled with their gene name. Genes whose proteins were differentially expressed in the surface proteomics dataset are noted in blue and labeled with their protein name. B. Expression level from the single-cell transcriptomics dataset for secreted proteins identified by the cytokine array to have increased abundance in iTF-Microglia with *ADNP* KD (N = 236-293 cells, violin plot area represents the density curve, two-tailed Student's t-test).

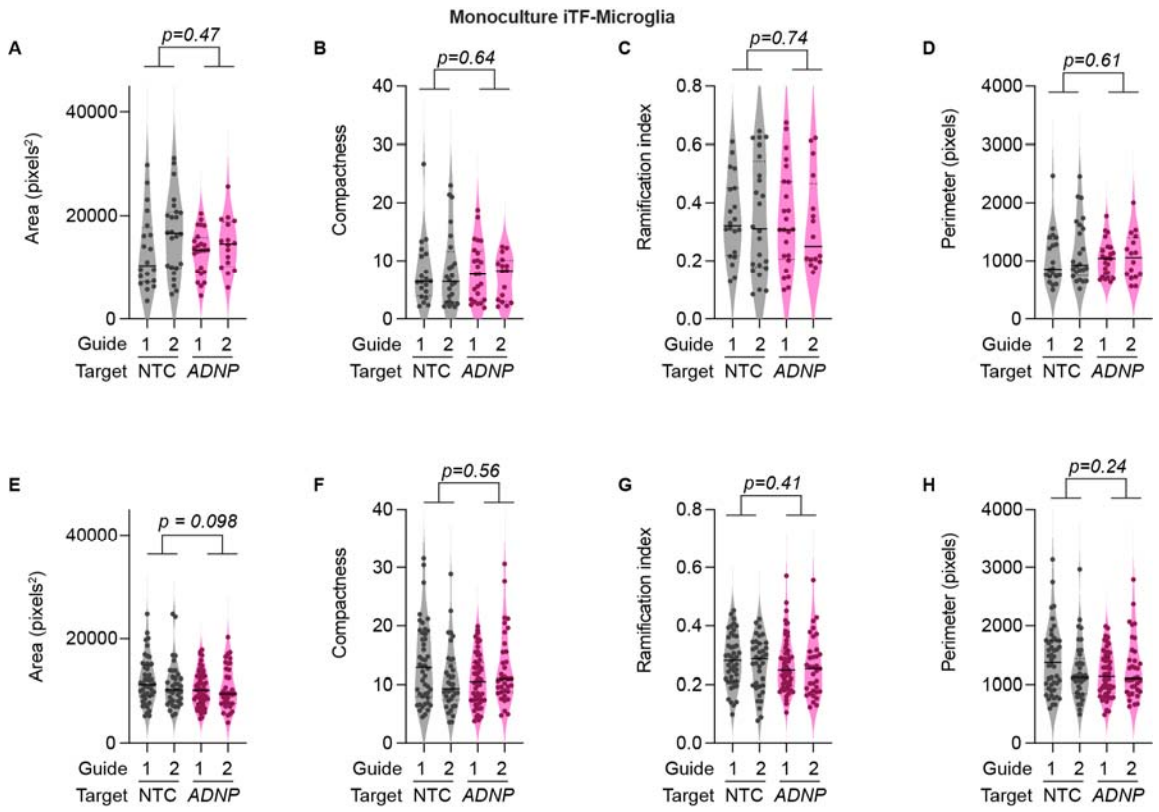

Supplementary Figure 5. iPSC-derived microglia (iTF-Microglia) morphology. A-D. Single cell morphology metrics for iTF-Microglia with *ADNP* KD or NTC in monoculture (N = 16-24 single cells, violin plot area represents the density curve, median and quartiles noted as bold and dashed lines respectively, two-way ANOVA). E-H. Single cell morphology metrics for iTF-Microglia with *ADNP* KD or NTC in cococulture (N = 35-59 single cells, violin plot area represents the density curve, median and quartiles noted as bold and dashed lines respectively, significance based on NTC vs ADNP factor computed by two-way ANOVA).

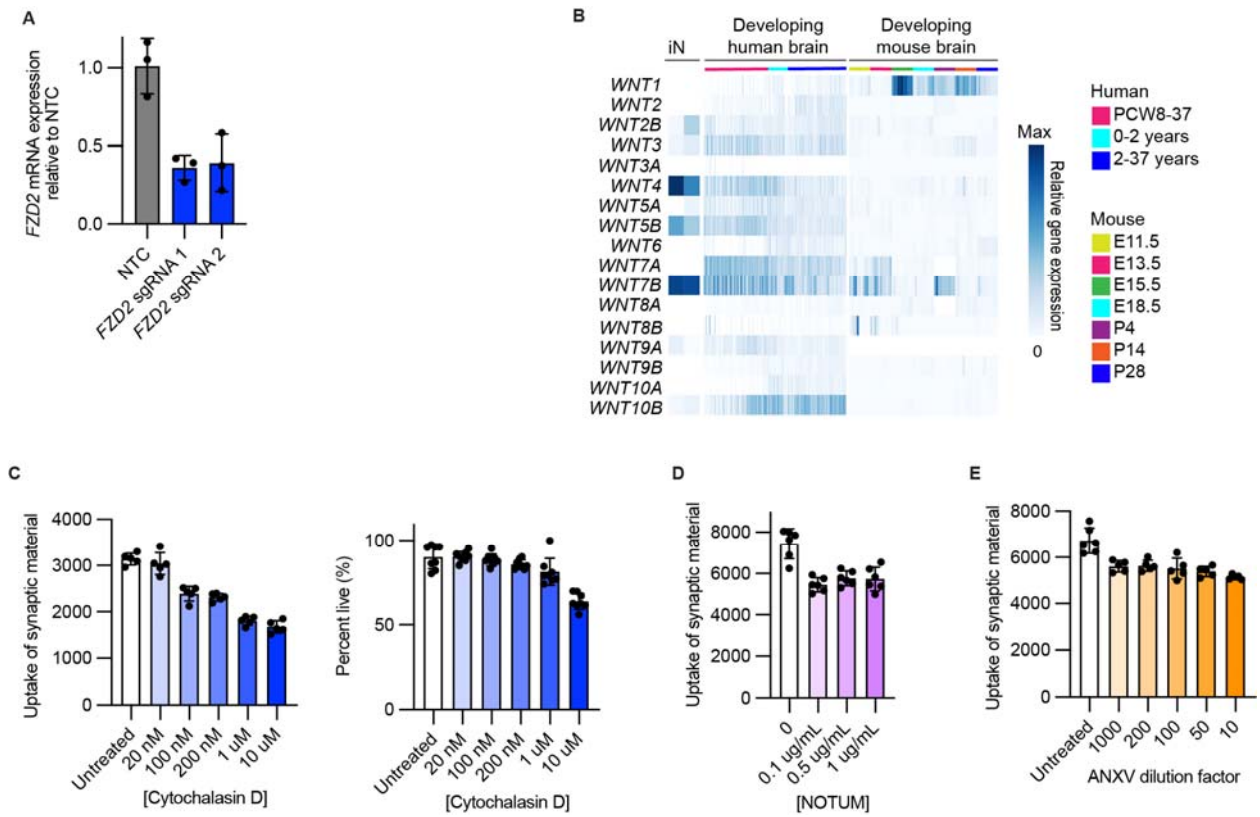

Supplementary Figure 6: Characterization of WNT signaling components in the iPSC-derived neuron (iNeuron) and iPSC-derived microglia (iTF-Microglia) coculture. A. *FZD2* mRNA expression in iTF-Microglia with sgRNAs targeting *FZD2* or non-targeting control (NTC) measured by qPCR B. Heatmap showing relative expression of WNT ligand genes by iNeurons in coculture compared to the developing human brains and, and expression of their homologs in mouse brains (from Brainspan, PCW = postconceptual weeks, E = embryonic day, P = postnatal day). C. (Left) Uptake of synaptic material by iTF-Microglia measured by flow cytometry after treating cocultures with increasing concentrations of cytochalasin D (N = 5 wells, bars represent mean +/- standard deviation). (Right) Percent live cells based on nuclear TO-PRO-3 intensity with increasing concentrations of cytochalasin D (N = 4 fields of view from 2 wells, bars represent mean +/- standard deviation). D. Uptake of synaptic material by iTF-Microglia measured by flow cytometry after treating cocultures with increasing concentrations of Notum (N = 6 wells, bars represent mean +/- standard deviation). E. Uptake of synaptic material by iTF-Microglia measured by flow cytometry after treating cocultures with decreasing dilutions of AnnexinV (N = 5-6 wells, bars represent mean +/- standard deviation).

Supplementary Movie 1: Synaptophysin-Gamillus trafficking in iPSC-derived neurons (iNeurons). iNeurons engineered to express synaptophysin-Gamillus were sparsely plated with unlabeled iNeurons. Individually engineered iNeurons show trafficking of synaptophysin-Gamillus puncta.

Supplementary Movie 2: iPSC-derived microglia (iTF-Microglia) engulf synaptophysin-Gamillus puncta. Labeled iTF-Microglia (gray) were cocultured with iPSC-derived neurons (iNeurons) engineered to express synaptophysin-Gamillus (green). iTF-Microglia can engulf synaptophysin-Gamillus puncta.

Supplementary Movie 3: iPSC-derived microglia (iTF-Microglia) traffick phagocytic cups containing synaptophysin-Gamillus. Labeled iTF-Microglia (gray) were cocultured with iPSC-derived neurons (iNeurons) engineered to express synaptophysin-Gamillus (green). iTF-Microglia traffick phagocytic cups containing synaptophysin-Gamillus puncta toward their soma.

Supplementary Table 1: sgRNA sequences targeting 102 ASD risk genes.

Supplementary Table 2: GO Cellular Component output for upregulated DEGs in Gandal 2022.

Supplementary Table 3: Raw cytokine array values for 30 secreted proteins.